PN-AB2-031
91378

Annual Report

April 1, 1995-March 31, 1996

An Intelligent Integrated Saltwater Intrusion Modelling System

Grant No. TA-MOU-94-C14-209/ TA-MOU-94-C14-209T

submitted to:
Agency for International Development
US-Israel Cooperative Development Research Program

Date of Submission:
July 1996

Submitted by:
The University of Delaware, USA
Tel-Aviv University, Israel

Address comments and inquiries to:

Dr. Alexander H-D. Cheng
U.S. Project Coordinator
Water Resources Program
Department of Civil Engineering
University of Delaware
Newark, Delaware 19716-3120
USA

Tel: (302)831-6787
Fax: (302)831-3640
Email: cheng@chaos.ce.udel.edu
WWW: http://www.ce.udel.edu/faculty/cheng/

Prof. Gedeon Dagan
Dept. Fluid Mechanics & Heat Transfer
Faculty of Engineering
Tel-Aviv University
P.O. Box 39040
Ramat-Aviv, Tel-Aviv 69978
Israel

Tel: 972-3-545-0930
Fax: 972-3-642-9540
Email: dagan@eng.tau.ac.il

Executive Summary

The project was launched by a coordination meeting in Morocco in April 1995 by the three collaborating scientists—Gideon Dagan of Israel, Driss Ouazar of Morocco, and Alexander Cheng of US. Basic research plan was drawn in that meeting. From July to September, 1995, Ouazar visited Delaware to collect literature worked with Cheng. During September, 1995, Ismael Herrera of Mexico visited Delaware to work with both Ouazar and Cheng. During March, 1996, Ouazar and Cheng visited Israel to meet with Dagan and Zeitoun to update each other the progress of the research. Throughout the year, close communication was maintained utilizing the e-mail facility.

Two technical reports are developed and attached in this Annual Report. The first one investigates the problem of a sharp interface between salt and fresh waters in an aquifer of spatially variable permeability. Layered structure, with permeability a stationary random function of the vertical coordinate, of given mean and two point covariance, is considered. Exact analytical solution of two-dimensional steady flow of fresh water in a confined aquifer, with salt water in rest, is derived. Also, the uncertainty of the discharge of a coastal collector, for a given depth of the upconed interface, is examined. By using conditional probability, the impact of measurement of the interface depth in a given cross-section, on the reduction of the uncertainty of its position, is determined. The second problem investigated is the generalization of Keulegan solution of unsteady flow that results from an abrupt removal of a thin vertical partition between salt and fresh water bodies.

In the second report, the location of sharp interface between salt and freshwater in coastal aquifer is determined using optimization techniques. The algorithm is based on the combination of a nonlinear programming and an *h*-adaptive boundary element method. The objective is to create to an automated solution procedure. The effectiveness of the model is demonstrated using several examples in confined and unconfined aquifers. The unconfined aquifer cases require the simultaneous determination of an interface and a free surface.

Section I

A. Research Objectives

Replaced by Technical Report (Appendices I and II).

B. Research Accomplishment

Replaced by Technical Report (Appendices I and II).

C. Scientific Impact of Collaboration

The work was divided into two parts according to the specialties of the teams. The Israeli team tackles the analytical part first. The work will be transferred to the Moroccan team for software development. The Moroccan team works on the numerical method. Later on, the stochastic theory developed by the Israeli team will be implemented to the numerical model.

D. Project Impact

Since we are still at the intermediate stage of the project, the results are not yet being used by the public.

E. Strengthening of Developing Country Institution

The Moroccan Investigator, Driss Ouazar spend two months in the US to enrich his knowledge in saltwater intrusion. A bibliography search was conducted utilizing the University of Delaware Library. A large volume of references were collected and brought back to Morocco. A Pentium computer was purchased and shipped back to Morocco.

F. Future Work

Future work include the continuing development of the theoretical work on the tracking of the stochastic location of salt/fresh water interface by the Israeli team, the field data collection and software development by the Morocco team. The project is roughly on schedule.

Section II

A. Managerial Issues

The project progresses as planned. There was no special managerial issue that occurred during this period.

B. Budget

No major change of budget during this period.

C. Special Concerns

None during this period.

D. Collaboration, Travel and Training

The project was launched in April 1995 following a coordination meeting in Morocco by the three collaborating scientists—Gideon Dagan of Israel, Driss Ouazar of Morocco, and Alexander Cheng of US. In that meeting, the basic research plan was drawn. The three investigators then returned to their own home base to continue the research. E-mail was utilized to frequently exchange information and update progresses.

From mid-July to mid-September, 1995, Ouazar visited Delaware to work closely with Cheng. Communication with Dagan was maintained via e-mail. During September, 1995, Ismael Herrera of Mexico visited Delaware to work with both Ouazar and Cheng. These have been reported in the semi-annual report.

During March, 1996, Ouazar and Cheng visited Israel to meet with Dagan to update the progress of the research. The following are some of the activities:

- A meeting was held on March 24, 1996, among Ouazar, Cheng, Dagan and Zeitoun at Tel Aviv University. Dr. Zeitoun is an expert in numerical modeling of saltwater intrusion. He was recruited by Dagan to conduct the computer programming part of the stochastic salt/fresh water interface tracking.
- On March 26, Ouazar and Cheng took a field trip to the Dead Sea Valley to understand the climate, hydrology, and water resources of Israel.
- On March 27, a meeting was held with Dr. Mulenex, Science Attaché, at the US Embassy, Tel Aviv. Present in the meeting ware Ouazar, Dagan, Cheng, Konikow (USGS) and Sorek (Ben-Gurion University). Dr. Mulenex was briefed about the project and the collaboration. He had made a few suggestions saltwater intrusion and other water resources related issues in Israel, Gaza Strip and West Bank.

4

- During the same day, the team visited the AID Mission at Tel Aviv. A meeting was held with Mr. John Starnes and his colleague. Technical information was exchanged.
- On March 28, 1996, Ouazar and Cheng took a field trip to the pumping station of the National Water Carrier. The trip continued to the Sea of Galilee, which was used as a fresh water reservoir for water supply in Israel, to Golan Height that served as the watershed of Galilee, and to the Yarmouk River basin.

During May 1996 Cheng visited Herrera in Mexico to consult some technical detail of saltwater intrusion modeling.

E. Request for USAID or BOSTID Actions

None during this period.

Seawater-freshwater interface in a stratified aquifer of random permeability distribution.

G. Dagan, D.G.Zeitoun
Faculty of Engineering, Tel Aviv University, Israel

Abstract

We consider the problem of a sharp interface between salt and fresh waters in an aquifer of spatially variable permeability. We assume a layered structure, with permeability a stationary random function of the vertical coordinate, of given mean and two point covariance. The flow is shallow and it obeys Dupuit assumption.

We derive an exact analytical solution of two-dimensional steady flow of fresh water in a confined aquifer, with salt water in rest. The mean interface shape is Dupuit parabola, for a constant effective permeability equal to the arithmetic mean of the variable one. The variance of the interface coordinate, and particularly of the toe, depends on the permeability variance and integral scale. The uncertainty of the interface location can be quite large. We also investigate the uncertainty of the discharge of a coastal collector, for a given depth of the upconed interface. We also determine, by using conditional probabality, the impact of measurement of the interface depth in a given cross-section, on the reduction of the uncertainty of its position.

The second case is the generalization of Keulegan (1954) solution of unsteady flow that results from an abrupt removal of a thin vertical partition between salt and fresh water bodies. The mean interface is similar to that prevailing in a homogeneous medium, i.e. a rotating line whose slope is approximately corresponding to the permeability arithmetic mean. The uncertainty affecting the interface position is of a smaller extent than that in steady flow.

6

1 INTRODUCTION

Models of salt and fresh waters flow in coastal aquifers serve as important tools for assessing the extent of salt water intrusion in coastal aquifers and for planning the rational exploitation of water resources. In a few circumstances the seawater is separated from the overlaying fresh water body by a relatively narrow zone which can be approximated by a sharp interface. Then, the aim of modeling is to determine the shape of the interface and the flow field in the two water bodies.

A few mathematical approaches have been developed in the past in order to solve the equations of flow and transport. The first, and most general, regards the entire fluid as one of variable density which depends on salt concentration. The system of equations governing the process are Darcy's law, conservation of mass and the equation of transport of salt regarded as a solute. Examples of numerical solutions of such a system are those of Segol and Pinder (1976) for 2D and Huyakorn et al (1987) for 3D. This approach is of great numerical complexity and it faces difficulties in modeling the transition zone, of high concentration gradients. Furthermore, it may affected by numerical dispersion which leads to excessive mixing.

In the second category of solutions, a sharp interface approximation is adopted and the basic equations are Darcy's Law, mass conservation in the two fluids and continuity of pressure across the interface. The ensuing problem of a free boundary is still a nonlinear, difficult, one. A few analytical solutions were obtained in the past for steady flow, e.g. Henry (1959) and Bear and Dagan (1964a), or by linearization, Dagan and Bear (1968). A few examples of more general, numerical, solutions are those of Mercer et al (1980), Liu et al (1981) and Taigbenu et al (1984).

The third and simplest approach is the one adopting the additional Dupuit assumption, of hydrostatic pressure distribution along the vertical in each fluid, applying to the case of a shallow interface. Its well known consequence is the Ghyben-Herzberg relationship (see, e.g. Bear, 1979) between the fresh water head and the depth of the interface in steady flow. The unsteady flow problem is still nonlinear and besides a simple analytical solution obtained by Keulegan (1954), numerical procedures, e.g. Shamir and Dagan (1971) and Wilson and Da Costa (1982), have to be adopted.

All the above solutions were applied to homogeneous formations or to heterogeneous ones made up from a few distinct units of well defined properties. Thus Rumer and Shiau (1968) and Mualem and Bear (1974) have

considered stratified aquifers of a few horizontal layers of, given, contrasting permeabilities.

Actual formations are known to display spatial variability of their properties. Thus, the permeability is generally found to change by orders of magnitude and in an irregular manner in space over scales much larger than the pore-scale. Heterogeneity has been shown to play an important role in transport of solutes, leading to "macrodispersion". To account for this seemingly erratic variation and the uncertainty affecting its values, the common approach is to regard permeability as random and to characterize it statistically. This randomness propagates to the flow variables and concentrations through the equations of flow and transport, which are of a stochastic nature (see, e.g. Dagan, 1989). Astonishingly enough, no attempt has been made so far, to our best knowledge, in order to investigate the effect of random heterogeneity upon seawater intrusion. The present study constitutes such an attempt and it treats two relatively simple problems which have been solved analytically in the past for homogeneous formations.

Our basic assumption is that heterogeneity manifests in perfect layering, with permeability a random function of depth. This picture agrees with most field findings for sedimentary aquifers, which are made from thin lenses of different depositional characteristics. Generally, layering is not perfect in the horizontal direction, but as far as the interface shape is concerned, the effect of the assumption is presumably small if the anisotropy ratio is sufficiently small. We also adopt the Dupuit assumption, which may be valid for shallow flow and interface of mild slope.

Under these conditions we solve first the problem of steady fresh water flow above a body of immobile salt water (in a homogeneous aquifer the interface shape is the Dupuit parabola) for which we get an exact analytical solution. Subsequently we address the unsteady problem of Keulegan (1954) of a rotating interface in an otherwise quiescent fluid.

Our twofold aim is to acquire some basic understanding of the effect of heterogeneity on one hand and to obtain a few simple results of immediate application to field problems on the other hand.

8

2 MATHEMATICAL FORMULATION OF THE PROBLEM

We consider an aquifer of thickness D (Fig. 1), bounded by an impervious horizontal bottom at $z = 0$ and an impervious top layer at $z = D$, while x is an inland horizontal coordinates. With $z = \xi(x,t)$ the equation of the interface, Darcy's law for the horizontal components of the specific discharges reads

$$q_f = -K_f(z)\frac{\partial \Phi_f}{\partial x} \qquad (\xi < z \leq D) \tag{1}$$

$$q_s = -K_s(z)\frac{\partial \Phi_s}{\partial x} \qquad (0 \leq z < \xi) \tag{2}$$

where $\Phi_f = p_f/\rho_f g + z$ and $\Phi_s = p_s/\rho_s g + z$ are the pressure heads, p is the pressure, ρ is density and K is the hydraulic conductivity. Here and in the sequel the indices f and s stand for fresh and salt water, respectively.

The hydraulic conductivities may be written in terms of the permeability k, the dynamic viscosity μ and the fluid density ρ as follows

$$K_f(z) = \frac{k(z)\,\rho_f}{\mu_f} \;\; ; \;\; K_s(z) = \frac{k(z)\,\rho_s}{\mu_s} \tag{3}$$

with k modeled as a stationary random function of z. We express it as $k(z) = k_A[1 + \mathcal{K}(z)]$ where $k_A = \langle k \rangle$ represents the constant arithmetic mean and $\mathcal{K}(z) = [k(z) - k_A]/k_A$ is the normalized fluctuation. Thus, at second order $\mathcal{K}$ is characterized by

$$\langle \mathcal{K}(z) \rangle = 0 \;\; ; \;\; \langle\, \mathcal{K}(z_1)\mathcal{K}(z_2) \rangle = \sigma^2\, r(z_1 - z_2) \;\; ; \;\; I = \int_0^\infty r(z)dz \tag{4}$$

where the brackets $\langle\ \rangle$ denotes ensemble averaging, $\sigma^2 = \sigma_k^2/k_A^2$ is the variance and $r(z)$ is the autocorrelation of $\mathcal{K}$, while I is its integral scale. The total discharges in the freshwater zone Q_f and in the saltwater zone Q_s are obtained by integrating (1) and (2) over each domain as follows

$$Q_f = \int_\xi^D q_f(z)dz = -K_{Af}[D - \xi + \int_\xi^D \mathcal{K}(z)dz]\frac{\partial \Phi_f}{\partial x} \tag{5}$$

$$Q_s = \int_0^\xi q_s(z)dz = -K_{As}[\xi + \int_0^\xi \mathcal{K}(z)dz]\frac{\partial \Phi_s}{\partial x} \tag{6}$$

9

where $K_{Af} = k_A\, g\, \rho_f/\mu_f$ and $K_{As} = k_A\, g\, \rho_s/\mu_s$. The mass conservation of the incompressible fluid in each zone of the confined aquifer yields

$$n\frac{\partial \xi}{\partial t} = \frac{\partial Q_f}{\partial x} = -\frac{\partial Q_s}{\partial x} \tag{7}$$

where n is the constant porosity. Finally, the pressure continuity at the interface $p_f(x,\xi,t) = p_s(x,\xi,t)$ yields by the definition of the pressure heads

$$\xi = \frac{\rho_s}{\rho_s - \rho_f}\Phi_s - \frac{\rho_f}{\rho_s - \rho_f}\Phi_f \tag{8}$$

Dupuit assumptions implies that the heads are independent of z, i.e. $\Phi_f = \Phi_f(x,t)$ and $\Phi_s = \Phi_s(x,t)$. Generally, substitution of (5), (6) and (8) in (7) yields two nonlinear partial differential equations for Φ_f and Φ_s that have to be solved with appropriate initial and boundary conditions while ξ is given by (8). Instead, we consider here simpler cases in which the interface expression can be determined directly from an unique partial differential equation (see, e.g. Bear and Dagan, 1964b for a homogeneous aquifer). Denoting by $Q(t) = Q_f(x,t) + Q_s(x,t)$ the total given discharge of the fluid, which according to (7) is a function of t solely, leads with the aid of (5) and (6) to

$$\begin{aligned} K_{Af}\, J(\xi,D)\,\frac{\partial \Phi_f}{\partial x} + K_{As}\, J(0,\xi)\,\frac{\partial \Phi_s}{\partial x} &= -Q(t) \quad \text{where for brevity} \\ J(a,b) &= b - a + \int_a^b \mathcal{K}(z)\,dz \end{aligned} \tag{9}$$

Differentiation of (8) with respect to x and insertion of $\partial\Phi_s/\partial x$ (9) leads to expressions of $\partial\Phi_f/\partial x$ and $\partial\Phi_s/\partial x$ in terms of $\partial\xi/\partial x$. Subsequently, substitution in Q_f and Q_s (5,6) and of the latter in (7) yields the following equation for $\xi(x,t)$

$$n\frac{\partial \xi}{\partial t} = \frac{\partial}{\partial x}\left[\frac{1}{A(\xi)+B(\xi)}\frac{\partial \xi}{\partial x}\right] + Q(t)\frac{\partial}{\partial x}\left[\frac{A(\xi)}{A(\xi)+B(\xi)}\right] \tag{10}$$

where

$$A(\xi) = \frac{\rho_s}{(\rho_s-\rho_f)K_{As}}\frac{1}{J(0,\xi)} \quad ; \quad B(\xi) = \frac{\rho_f}{(\rho_s-\rho_f)K_{Af}}\frac{1}{J(\xi,D)}$$

For a homogeneous aquifer, i.e. $\mathcal{K} \equiv 0$, $J(0,\xi) = \xi$, $J(\xi,D) = D - \xi$, we recover the previous formulation of Bear and Dagan (1964b).

10

We shall show in the sequel that in the case of a heterogeneous aquifer it is advantageous to express the interface equation in the explicit form $x = \chi(z,t)$ rather than $z = \xi(x,t)$. By using the relationships between derivatives

$$\frac{\partial \chi}{\partial z}\frac{\partial \xi}{\partial x} = 1 \; ; \; \frac{\partial \chi}{\partial z}\frac{\partial \xi}{\partial t} = -\frac{\partial \chi}{\partial t} \tag{11}$$

we get in (10)

$$n\frac{\partial \chi}{\partial t} = \frac{\partial}{\partial z}[\frac{1}{A(z)+B(z)}(\frac{\partial \chi}{\partial z})^{-1}] - Q(t)\frac{\partial}{\partial z}[\frac{A(z)}{A(z)+B(z)}] \quad (0 \leq z \leq D) \tag{12}$$

The dynamical viscosity of the fresh water is slightly different from that of the salt water, i.e. $\mu_s \simeq \mu_f$, and Eq. (12) can be further simplified by using the single parameter for the mean hydraulic conductivity $K" = (\rho_s - \rho_f)K_{Af}/\rho_f \cong (\rho_s - \rho_f)K_{As}/\rho_s$. Substitution in A, B (10) yields the final form of the equation satisfied by $\chi(x,t)$

$$\frac{n\,J(0,D)}{K"}\frac{\partial \chi}{\partial t} = -\frac{\partial}{\partial z}[\frac{J(0,z)\,J(z,D)}{\partial \chi/\partial z}] - \frac{Q(t)}{K"}\frac{\partial J(0,z)}{\partial z} \qquad (0 \leq z \leq D \quad ; t \geq 0) \tag{13}$$

where it is reminded that $J(a,b) = b - a + \int_a^b \mathcal{K}(z)\,dz$.

The stochastic partial differential equation (13), supplemented by appropriate initial boundary and initial conditions, and for given statistical moments of $\mathcal{K}$, constitutes the starting point for obtaining solutions of the interface motion in the sequel.

3 STEADY STATE SOLUTION

3.1 General

We consider first the simplest case of salt water under rest, i.e. $\Phi_s = const$, and a steady interface, i.e. $\partial\chi/\partial t = 0$. In this case $Q = const$ and from (13) we get

$$\frac{d}{dz}[J(0,z)\,(\frac{J(z,D)}{d\chi/dz} + \frac{Q}{K"})] = 0 \qquad (0 \leq z \leq D) \tag{14}$$

Since at $z = 0$, $J(0,z) = z + \int_0^z \mathcal{K}(z')\,dz' = 0$, integration in (14) yields the general solution

$$\frac{d\chi}{dz} = -\frac{K"}{Q}[D - z + \int_z^D \mathcal{K}(z')\,dz'] \tag{15}$$

Consistent with Dupuit assumption we neglect the seepage face and assume that the interface originates at $x = 0, z = D$, i.e. the sea serves as a sink (Fig. 1), and the boundary condition is $\chi(D) = 0$. This approximation becomes accurate for a shallow interface, i.e. for $\chi(0) > D$ (see, Bear and Dagan, 1964a).

With the change of variable $\zeta = D - z$ (see figure 1) and after integration of the last equation with $\chi(0) = 0$, the exact solution for the random $\chi(\zeta)$ may be written as follows

$$\chi(\zeta) = \frac{K"}{Q}[\frac{\zeta^2}{2} + \int_0^\zeta d\zeta' \int_0^{\zeta'} \mathcal{K}(\zeta")\,d\zeta"] \quad where\ K" = \frac{\rho_s - \rho_f}{\rho_f} K_{Af} \tag{16}$$

Eq. (16) permits one to compute the various moments of the nonstationary random function $\chi(\zeta)$. Thus, ensemble averaging of (16) yields for the average position of the interface

$$\langle\chi(\zeta)\rangle = \frac{K"}{Q}\frac{\zeta^2}{2} \tag{17}$$

which is precisely the Dupuit parabola obtained previously for a homogeneous medium, provided the constant hydraulic conductivity is taken equal with K_{Af}. This is consistent with the well known result that for flow parallel to the bedding the effective permeability is the arithmetic mean.

The autocovariance $C_\chi(\zeta_1, \zeta_2) = \langle[\chi(\zeta_1) - \langle\chi(\zeta_1)\rangle][\chi(\zeta_2) - \langle\chi(\zeta_2)\rangle]\rangle$ is obtained by subtracting first (17) from (16) and ensemble averaging the product of χ fluctuations, leading to

$$C_\chi(\zeta_1, \zeta_2) = \sigma^2 (\frac{K"}{Q})^2 \int_0^{\zeta_1} \int_0^{\zeta_2} \int_0^{\zeta'} \int_0^{\zeta"} r(u - v)\,du\,dv\,d\zeta'\,d\zeta" \tag{18}$$

It is reminded that by (4) σ^2 and r are the variance and autocorrelation of $\mathcal{K}(\zeta)$, respectively. The variance of χ is given by $\sigma_\chi^2(\zeta) = C_\chi(\zeta, \zeta)$ and the mean position of the toe of the interface and its variance are $\langle\chi(D)\rangle = (K"\,D^2/2\,Q)$ and $\sigma_\chi^2(D) = C_\chi(D, D)$, respectively.

These general results are applied next to a few typical problems encountered in practice.

12

3.2 Applications

The interpretation of the results of the previous subsection is that in a stratified aquifer of random permeability distribution the interface deviates from its mean value and its shape cannot be predicted in a deterministic manner in the given realization, but only in terms of probability. It is, therefore, important to establish an interval of confidence for the interface location (Fig. 2). Toward this aim we select a particular permeability covariance function

$$r(\zeta) = \exp(-|\zeta|/I) \tag{19}$$

To simplify notations we introduce the dimensionless variables $\chi' = \chi/D$, $\zeta' = \zeta/D$, $Q" = Q/K"D = (Q\,\rho_f)/[K_{Af}(\rho_s - \rho_f)]$ and $I' = I/D$. It is seen that $\langle\chi'\rangle = \zeta'^2/2Q"$ (17) and $C_{\chi'}$ (18) depend on the dimensionless parameters $\sigma = \sigma_k/k_A$, $I' = I/D$ and $Q"$.

Substitution of (19) in (18) leads to the following close form expression of C_χ

$$C_{\chi'}(\zeta_1', \zeta_2') = \frac{\sigma^2 I'^4}{Q"^2}[-\frac{1}{3}(\frac{\zeta_1'}{I'})^3 + (\frac{\zeta_1'}{I'})^2\frac{\zeta_2'}{I'} - \frac{\zeta_1'}{I'}\frac{\zeta_2'}{I'} + \frac{\zeta_2'}{I'} - \frac{\zeta_1'}{I'} + 1 \tag{20}$$

$$-\frac{\zeta_2'}{I'}e^{-\zeta_1'/I'} - \frac{\zeta_1'}{I'}e^{-\zeta_2'/I'} + e^{(\zeta_1'-\zeta_2')/I'} - e^{-\zeta_2'/I'} - e^{-\zeta_1'/I'}] \quad (\zeta_1' \leq \zeta_2')$$

In particular the variance of the interface horizontal coordinate is given by

$$\sigma^2_{\chi'}(\zeta') = C_{\chi'}(\zeta, \zeta) = \frac{\sigma^2 I'^4}{Q"^2}[\frac{2}{3}(\frac{\zeta'}{I'})^3 - (\frac{\zeta'}{I'})^2 - 2(\frac{\zeta'}{I'})\,e^{-\zeta'/I'} - 2\,e^{-\zeta'/I'} + 2] \quad (0 \leq \zeta' \leq 1) \tag{21}$$

To illustrate this results we further assume that k is lognormal and with $Y = \ln k$ we have $\sigma^2 = \exp(\sigma_Y^2) - 1$. Then, the coefficient of variation is given by

$$CV_\chi(\zeta') = \sigma_{\chi'}/\langle\chi'\rangle = 2I'^2\{[\exp(\sigma_Y^2) - 1][\frac{2}{3}(\frac{\zeta'}{I'})^3 - (\frac{\zeta'}{I'})^2 - 2(\frac{\zeta'}{I'})\,e^{-\zeta'/I'} - 2\,e^{-\zeta'/I'} + 2]\}^{1/2}/\zeta'^2 \tag{22}$$

13

As a first application, we consider the problem of predicting the shape of the interface for given D, Q, ρ_s, ρ_f, K_{Af}, σ_Y^2 and I. The best we can do is to determine the mean profile (17) and the interval of confidence (22). To illustrate the results we have depicted in Fig. 2 $\langle\chi'(\zeta')\rangle$ and $\langle\chi'(\zeta')\rangle \pm 2\sigma_{\chi'}$ for the following parameters values: the mean toe $\langle\chi'(1)\rangle = 3$, $\sigma_Y^2 = 1$ and $I' = 0.01$. The small value of $I' = I/D$ is consistent with the assumption that the statistical moments of $Y = \ln k$ can be identified from the available aquifer data, say by analyzing measurements of conductivity values from a well. In particular, the coefficient of variation of the toe location (22) for such a small I' is approximately equal to $CV_\chi(1) \cong [8(e^{\sigma_Y^2} - 1)I/3D]^{1/2} = 0.21$ (Fig. 2) and the uncertainty is quite large.

Another application of interest is related to pumping of fresh water above the interface (Fig. 3) by a "coastal collector" located at $x = x_d$. We assume that out of a total fresh-water discharge Q a portion Q_d is drained, leaving $Q_s = Q - Q_d$ to flow to the sea and as a result the interface raises at a depth ζ_d (Fig. 3). The relevant question in this case is what is the maximum available Q_d provided that the interface does not raise above $\zeta = \zeta_d$. An appropriate model has to take into account the fact that pumping is carried out by a drain or by wells, which create a local upconning (see the recent discussion in Journal of Contaminant Hydrology, 18, 319-339, 1995). Nevertheless, within the limitations of Dupuit assumption, we wish to answer this question in a stochastic framework, for a random stratified aquifer. Thus, we recast Eq. (16) in the following form

$$\frac{Q_s}{K"} = \frac{[\zeta_d^2/2 + \int_0^{\zeta_d} d\zeta' \int_0^{\zeta'} \mathcal{K}(\zeta")\, d\zeta"]}{x_d} \tag{23}$$

relating the random discharge Q_s to the given interface depth ζ_d at $\chi = x_d$, for a random permeability field. From (23), for an exponential r (19) and by analogy with (16) we obtain for the dimensionless $Q_s' = Q_s/K"D$

$$\langle Q_s'\rangle = \frac{\zeta_d'^2}{2\,x_d'} \quad ; \quad \frac{\sigma_{Q_s}}{\langle Q_s\rangle} = CV_\chi(\zeta_d') \tag{24}$$

where CV_χ is given by (22). To illustrate the results we have depicted in Fig. 4 the dependance of $\langle Q_s'\rangle \pm 2\sigma_{Q_s'}'$ on ζ_d' for the same parameters values as in Fig. 2. It is seen that the fresh-water discharge to the sea is affected by relatively large uncertainty, depending on the location of the collector.

Finally, we consider the prediction of the interface location for given $Q, D, K_{Af}, \rho_s, \rho_f$ and I, supplemented by a measurement of ζ_1 at a given

14

$x = x_1$. This is the case in which, besides the information on the fresh-water discharge to the sea and on the statistics of k, we also measure the interface depth in a given cross-section by a piezometer. We treat this problem in the context of conditional probability, our aim being to determine $\langle \chi^c(\zeta|\zeta_1)\rangle$ and $\sigma_\chi^{c,2}(\zeta|\zeta_1)$, the conditional mean and variance of the interface coordinate χ as function of ζ, given the measurement of ζ_1. This is not a simple task since χ (16) is neither a stationary random function nor one of stationary increments. We shall use the conditioning relationships, similar to kriging, that apply to normal residuals (see, e.g. Dagan, 1989) and are not restricted by stationarity. This approximation is justified at least for $\zeta \gg I$, since by the central limit theorem χ (16) tends to normality. Hence, we may write in the more general case of conditioning by $\zeta_1, \zeta_2, ..., \zeta_N$ measurements

$$\langle \chi^c(\zeta|\zeta_1, \zeta_2, ..., \zeta_N)\rangle = \langle \chi(\zeta\rangle + \sum_{j=1}^{N} \lambda_j \left[x_j - \langle \chi(\zeta_j)\rangle\right]$$

$$\sigma_\chi^{c,2}(\zeta|\zeta_1, \zeta_2, ..., \zeta_N) = \sigma_\chi^2(\zeta) - \sum_{j=1}^{N}\sum_{m=1}^{N} \lambda_j \lambda_m C_\chi(\zeta_j, \zeta_m) \tag{25}$$

$$\sum_{j=1}^{N} \lambda_j C_\chi(\zeta_j, \zeta_m) = C_\chi(\zeta, \zeta_m)$$

where the unconditional $\langle \chi\rangle$ and C_χ are given by (17) and (21), respectively. For the sake of illustration we consider $N = 1$, leading in (25) to

$$\begin{aligned} \lambda &= \frac{C_\chi(\zeta, \zeta_1)}{\sigma_\chi^2(\zeta_1)} \\ \langle \chi^c(\zeta|\zeta_1)\rangle &= \langle \chi(\zeta\rangle + \frac{C_\chi(\zeta, \zeta_1)}{\sigma_\chi^2(\zeta_1)}[x_1 - \langle \chi(\zeta_1)\rangle] \\ \sigma_\chi^{c,2}(\zeta|\zeta_1) &= \sigma_\chi^2(\zeta) - \frac{C_\chi^2(\zeta, \zeta_1)}{\sigma_\chi^2(\zeta_1)} \end{aligned} \tag{26}$$

To illustrate the results we consider the impact of a measurement upon the mean interface profile in Fig. 5, the parameters being the same as before, i.e. $\langle \chi'(1)\rangle = 3, I' = 0.01, \sigma = 1$, with conditioning at $x'_d = 1$, $\zeta'_1 = 0.4$. As expected from (26) the mean interface passes through the conidtioning

15

point while $\sigma_\chi^{c,2}(\zeta_1|\zeta_1) = 0$. However, the more interesting application is the reduction of uncertainty of the toe location, i.e. the ratio $\sigma_\chi^{c,2}(D|\zeta_1)/\sigma_\chi^2(D)$ which is represented in Fig. 6 as function of ζ_1' for the same parameters values as in the previous figures. The impact of a measurement upon variance reduction of toe location becomes more siginificant as the toe cross-section is approached. For the largest $I' = I/D = 0.1$ considered, the conditional variance is practically zero when $\zeta_1' \geq 0.5$. This effect is related in principle to the fact that for such large correlation scales, measurements affect a large interval of ζ. Furthermore, the uncoditional variance (18) "builds up" as one moves upstream from the sea boundary in a nonlinear manner.

4 UNSTEADY FLOW (GENERALIZATION OF KEULEGAN SOLUTION).

Keulegan (1954) has derived one of the few analytical existing solutions of unsteady interface flow. The case is that of an initial vertical interface separating quiescent salt and fresh water bodies. This can be visualized as the result of the abrupt removal of a thin partition separating the two fluids. The well known solution, to be recovered below, is of a rotating planar interface (Fig. 7). While Dupuit assumption is bound to be violated at small time, it is becoming increasingly valid as the interface slope becomes milder.

Our aim is to generalize this solution for the case of a nonhomogeneous, layered, aquifer of random permeability. The starting point is the general Equation (13) for $Q(t) = 0$, pertinent to fluids in rest far from the origin, i.e.

$$\frac{n}{K"}\frac{\partial \chi}{\partial t} = -\frac{\partial}{\partial z}\left[\frac{J(0,z)\,J(z,D)}{J(0,D)\,\partial\chi/\partial z}\right] \tag{27}$$

To simplify notations and computations we introduce the following dimensionless variables: $\chi' = \chi/D$, $t' = tK"/nD = tK_{Af}(\rho_s - \rho_f)/\rho_f nD$ and $\eta = (2z/D) - 1$. Then, Eq. (27) becomes

$$4\frac{\partial \chi'}{\partial t'} = -\frac{\partial}{\partial \eta}\left[\frac{C(\eta)}{\partial \chi'/\partial \eta}\right] \qquad (t' \geq 0, -1 \leq \eta \leq 1) \tag{28}$$

$$C(\eta) = \frac{[1 + \eta + \int_{-1}^{\eta} \mathcal{K}(u)\,du][1 - \eta + \int_{\eta}^{1} \mathcal{K}(u)\,du]}{1 + (1/2)\int_{-1}^{1} \mathcal{K}(u)\,du}$$

16

Hence, the generalized Keulegan problem can be stated now mathematically as seeking the solution for the random function $\chi'(\eta, t')$ that satisfies (28) with initial condition $\chi'(\eta, 0) = 0$ and for given statistical moments of $\mathcal{K}(\eta)$.

A significant simplification of the problem is achieved by the separation $\chi'(\eta, t') = \sqrt{t'}\, f(\eta)$, suggested by the Keulegan solution for a homogeneous medium. Substitution in (28) yields the ordinary differential equation $2f = -d/d\eta\,[C/(df/d\eta)]$. An additional integration, with $C(-1) = 0$ taken into account, leads to the nonlinear integro-differential equation

$$2\frac{df}{d\eta}\int_{-1}^{\eta} f(\eta')\,d\eta' = -C(\eta) \tag{29}$$

which has to be solved for the random $C(\eta)$ (28). While (29) may serve as the starting point for numerical integration, we seek here simple, analytical, solutions. Toward this aim we expand $C(\eta)$ (28) in an asymptotic expansion in σ,the standard deviation of $\mathcal{K}$, as follows

$$\begin{aligned} C &= C_0 + C_1 + C_2 + \dots \quad ; \quad C_0 = 1 - \eta^2 \qquad (30)\\ C_1 &= (1+\eta)\int_{\eta}^{1}\mathcal{K}(u)\,du + (1-\eta)\int_{-1}^{\eta}\mathcal{K}(u)\,du - \frac{1}{2}(1-\eta^2)\int_{-1}^{1}\mathcal{K}(u)\,du \end{aligned}$$

$$\begin{aligned} C_2 &= \int_{-1}^{\eta}\int_{\eta}^{1}\mathcal{K}(u)\,\mathcal{K}(v)\,du\,dv - \frac{1}{2}(1+\eta)\int_{\eta}^{1}\int_{-1}^{1}\mathcal{K}(u)\,\mathcal{K}(v)\,du\,dv - \\ &\quad \frac{1}{2}(1-\eta)\int_{\eta}^{1}\int_{-1}^{1}\mathcal{K}(u)\,\mathcal{K}(v)\,du\,dv + \frac{1}{4}(1-\eta^2)\int_{-1}^{1}\int_{-1}^{1}\mathcal{K}(u)\,\mathcal{K}(v)\,du\,dv \end{aligned}$$

In a similar manner, we expand the solution $f = f_0 + f_1 + f_2 + \dots$, where $f_0 = \mathrm{O}(1)$, $f_1 = \mathrm{O}(\sigma)$, $f_2 = \mathrm{O}(\sigma^2)$,... Substitution of these expansions in (29) leads to linear differential equations for f_i $(i = 1, 2, \dots)$. Thus, we get at zero-order

$$2\frac{df_0}{d\eta}\int_{-1}^{\eta} f_0(\eta')\,d\eta' = \eta^2 - 1 \tag{31}$$

which has the exact solution $f_0 = -\eta$. This is precisely Keulegan (1954) solution for a homogeneous aquifer of conductivity K_A. Thus, $\chi_0' = \sqrt{t'}\, f_0(\eta)$ that can be rewritten in terms of the original variables as follows

$$\chi_0(z,t) = [\frac{4tK"}{nD}]^{1/2}(\frac{D}{2} - z) \quad ; \quad K" = \frac{K_{Af}\,(\rho_s - \rho_f)}{\rho_f} \tag{32}$$

and the interface is a straight line, rotating around $z = D/2$, the salt water being to the left (Fig. 5). In particular the toe advances as $\chi_0(0,t) = (tK"D/n)^{1/2}$.

With $f_0 = -\eta$ we get from (29, 30) the following sequence of linear integro-differential equations for f_i

$$(1-\eta^2)\,\frac{df_1}{d\eta} - 2\int_{-1}^{\eta} f_1(\eta')\,d\eta' \;=\; -C_1(\eta) \tag{33}$$

$$(1-\eta^2)\,\frac{df_2}{d\eta} - 2\int_{-1}^{\eta} f_2(\eta')\,d\eta' \;=\; E_2(\eta) \quad ; \quad E_2 = -C_2 - 2\frac{df_1}{d\eta}\int_{-1}^{\eta} f_1\,d\eta'$$

and we shall solve for these two terms only. Furthermore, we seek the first two statistical moments of f solely, given at $O(\sigma^2)$ by $\langle f\rangle = f_0 + \langle f_2\rangle$, $C_f(\eta_1,\eta_2) = \langle f_1(\eta_1)\,f_1(\eta_2)\rangle$.

We have contemplated two methods to solve (33): a general one by using the Green function and its expansion in Legendre polynomials and a simpler, but more limited, one based on equations for the moments. While the first method is described in Appendix 1 for the sake of future applications, we shall follow here the second one. But first we rewrite (33) with the aid of the new variable $F(\eta) = \int_{-1}^{\eta} f(\eta')\,d\eta'$ as follows

$$(1-\eta^2)\,\frac{d^2F_1}{d\eta^2} - 2F_1 = -C_1 \quad ; \quad (1-\eta^2)\,\frac{d^2F_2}{d\eta^2} - 2F_2 = E_2 \tag{34}$$

and seek the moments $\langle F\rangle = F_0 + \langle F_2\rangle$, $C_F(\eta_1,\eta_2) = \langle F_1(\eta_1)\,F_1(\eta_2)\rangle$. Subsequently, we get $\langle f\rangle = \langle dF/d\eta\rangle$, $C_f(\eta_1,\eta_2) = \partial^2 C_F/\partial\eta_1\,\partial\eta_2$.

The pde satisfied by $C_F(\eta_1,\eta_2)$ is obtained by multiplying the equation (34) for $F_1(\eta_1)$ by the same equation for $F_2(\eta_2)$ and averaging . The result is

$$(1-\eta_1^2)(1-\eta_2^2)\,\frac{\partial^4 C_F}{\partial^2\eta_1\partial^2\eta_2} - 2(1-\eta_1^2)\,\frac{\partial^2 C_F}{\partial\eta_2^2} - 2(1-\eta_2^2)\,\frac{\partial^2 C_F}{\partial\eta_1^2} + 4C_F = C_{11}(\eta_1,\eta) \tag{35}$$

$$C_{11} \;=\; \langle C_1(\eta_1)\,C_1(\eta_2)\rangle$$

18

The complete expression of C_{11}, based on (30), is given in Appendix 2. It can be evaluated in a closed form for particular forms of the conductivity auto-correlation r, e.g. (19). We shall further limit the derivation to formations for which $I' = I/D \ll 1$, where I is the integral scale of r, and derive the leading order term of $\langle F \rangle$ and $\langle C_F \rangle$ in I'. This approximation allows us to derive general solutions, not necessarily related to a particular r. The simple result is obtained by replacing r, whenever it appears as an integrand, by $r(z_1 - z_2) = 2I\,\delta(z_1 - z_2)$ i.e. $r(\eta_1 - \eta_2) = 4I\,\delta(\eta_1 - \eta_2)$, where δ is the Dirac operator (Dagan, 1989). The final result (Appendix 2) is

$$C_{11} = 2\sigma^2 I'[1 - \eta_1^2 - \eta_2^2 + 4\eta_1\eta_2 - 4\eta_1\eta_2|\eta_1 - \eta_2| - 3\eta_1^2\eta_2^2] \qquad (36)$$

Next, we have to solve the pde (35) in order to derive C_F. Since the general solution (Appendix 1) can be expressed as an expansion of polynomials, and C_{11} (36) is a polynomial, it is natural to try for C_F a power series solution and to identify coefficients from (35). This results in the following exact solution of (35,36)

$$C_F = \frac{\sigma^2 I'}{2}[-\frac{3}{4} + 2|\eta_1 - \eta_2| - \frac{5}{4}\eta_1^2 - \frac{5}{4}\eta_2^2 + 4\eta_1\eta_2 - 2\eta_1\eta_2|\eta_1 - \eta_2| - \frac{3}{4}\eta_1^2\eta_2^2] \quad (37)$$

which can be checked by inspection.

The covariance $C_f(\eta_1, \eta_2)$ is obtained by differentiation of C_F. This poses a delicate problem along the line $\eta_1 = \eta_2$ in the η_1, η_2 plane, since the second derivative is discontinuous there, as a result of our replacement of the continuous r by a Dirac distribution. To obtain the correct value along the line of discontinuity, one has to average the two values of any function of interest across the line.

Hence, the solution for $C_f(\eta_1, \eta_2)$ and $\sigma_f^2(\eta) = C_f(\eta, \eta)$ are found as

$$C_f = \frac{\partial^2 C_F}{\partial\eta_1\partial\eta_2} = 2\sigma^2 I'\,[1 - |\eta_1 - \eta_2| - \frac{3}{4}\eta_1\eta_2] \;\; ; \;\; \sigma_f^2 = 2\sigma^2 I'\,(1 - \frac{3}{4}\eta^2) \quad (38)$$

Next, we seek the solution of $\langle F_2 \rangle$, after ensemble averaging (34), i.e. $(1 - \eta^2)\, d^2\langle F_2 \rangle / d\eta^2 - 2\langle F_2 \rangle = \langle E_2 \rangle$. It is shown in Appendix 2 that under the same approximation $\mathrm{O}(I')$ we have from (30) and (33)

$$\langle C_2 \rangle \;\; = \;\; -2\sigma^2 I'\,(1 - \eta^2) \;\; ; \;\; \langle \frac{df_1}{d\eta} \int_{-1}^{\eta} f_1\, d\eta' \rangle = \langle \frac{d^2 F_1}{d\eta^2} F_1 \rangle = -\frac{\sigma^2 I'}{4}(5 + 3\eta^2) \quad (39)$$

19

$$\langle E_2 \rangle \;=\; -\langle C_2 \rangle - 2\langle \frac{d^2 F_1}{d\eta^2} F_1 \rangle = \frac{\sigma^2 I'}{2}(9-\eta^2)$$

Once again, it is seen by inspection that the solution $\langle F_2 \rangle$ and the associated $\langle f_2 \rangle = d\langle F_2 \rangle / d\eta$ are given exactly by

$$\langle F_2 \rangle = \frac{\sigma^2 I'}{8}(-10+\eta^2) \quad ; \quad \langle f_2 \rangle = \frac{\sigma^2 I'}{4}\eta \tag{40}$$

Subsequently, we get at $\mathbf{O}(\sigma^2 I')$ by collecting results in (32, 38) and (40)

$$\langle f \rangle = f_0 + \langle f_2 \rangle = -(1-\frac{\sigma^2 I'}{4})\,\eta \quad ; \quad \sigma_f^2 = \sigma_f^2 = 2\sigma^2 I'\,(1-\frac{3}{4}\eta^2) \tag{41}$$

Finally, we have for the interface equation $x = \chi(z,t) = \sqrt{t'}\, f(z)$ in terms of the original variables

$$\begin{aligned} \langle \chi(z,t) \rangle \;&=\; [\frac{4tK"}{nD}]^{1/2}(1-\frac{\sigma^2 I}{4D})\,(\frac{D}{2}-z) \qquad (42) \\ \sigma_\chi^2 \;&=\; \frac{2\sigma^2 I K" t}{nD}[D^2 - 3(z-\frac{D}{2})^2] \;\; where \;\; K" = \frac{K_{Af}\,(\rho_s - \rho_f)}{\rho_f} \end{aligned}$$

The relationships (42) encapsulate the results of our analysis, generalizing Keulegan (1954) solution for a layered aquifer. In particular, we get for the toe location

$$\langle \chi(0,t) \rangle = [\frac{tK"}{nD}]^{1/2}(1-\frac{\sigma^2 I}{4D})D \quad ; \quad \frac{\sigma_\chi}{\langle \chi \rangle} = (\frac{\sigma^2 I}{2D})^{1/2} + \mathbf{O}(\sigma^2) \tag{43}$$

The generalized Keulegan solution (42, 43) does not lend itself to direct applications because of the particular boundary condition of zero net discharge. It may serve, however, as a benchmark for numerical codes. If we assume, nevertheless, that it is representative for more general cases of unsteady interface flows superimposed on the steady ones of the previous Section, we can draw the following conclusions for aquifers of small I/D and small to moderate $\sigma = \sigma_K/\langle K \rangle$: (i) the additional deviation of the mean interface profile is very slightly influenced by heterogeneity. For instance, for data similar to the ones adopted in the previous Section, i.e.

20

$\sigma^2 = 1$, $2I/D = 1/100$, the toe location is modified by 0.8%; (ii) the effective conductivity is practically the arithmetic mean and (iii) the additional uncertainty of the toe position is also small. Comparing it with that affecting it in the steady state (22) and for an equivalent thickness half of that of Keulegan's solution (Fig. 7), we find that coefficient of variation (43) is roughly three times smaller than the corresponding steady state value. These results suggest that the ones obtained for steady flow, under more general conditions, may be applicable approximately to unsteady flows as well. This conjectural conclusion has to be supported by future work of a numerical nature.

5 SUMMARY AND CONCLUSIONS

The present study is a first attempt to assess the influence of heterogeneity, related to the random spatial variability of permeability, on the shape of the interface between salt and fresh waters in coastal aquifers. To achieve simple results of an analytical nature, a few assumptions have been adopted: the existence of a sharp interface, shallow flow model (Dupuit assumption) and a layered structure with permeability a random and stationary function of depth only.

We have been able to arrive at an exact closed form solution for the statistical moments of the interface coordinate in two-dimensional steady flow of fresh-water to the sea. It generalizes the well-known Dupuit parabola for a homogeneous aquifer. We have found that the mean profile is the same parabola, provided the constant effective conductivity is taken equal to the arithmetic mean of the spatially variable one. The main finding, however, is the coefficient of variation of the interface coordinate and particularly that of the toe. This can be quite large, depending on the permeability variance and integral scale. Thus, prediction of interface shape and of salt water intrusion in heterogeneous aquifers is affected by uncertainty and our results permit one to determine the intervals of confidence. We have been able also to assess, by using conditional probability, the impact of measurements of interface position on reducing this uncertainty.

We have arrived at a generalization of Keulegan (1954) solution for unsteady flow caused by the sudden removal of a fictitious, vertical, partition between the two water bodies. An analytical solution has been obtained for the leading order term in the permeability variance and in the ratio between

21

the integral scale and the aquifer thickness. The mean interface is a rotating line, whose slope is influenced slightly by heterogeneity and whose coefficient of variation is smaller than for steady flow.

From a theoretical standpoint, many extensions of the present study that account for factors we neglected are possible, e.g. incorporating the effect of field scale pore-scale dispersion, of heterogeneity of a three-dimensional structure and solving for two- or three-dimensional flows for which Dupuit assumption does not apply. Such extensions may require, however, using more involved numerical methods.

From a field applications perspective it seems to us that assessing the impact of heterogeneity upon the interface shape by analyzing data on both permeability variability and interface location is of definite interest. The present results may, nevertheless, serve for rough estimates of the uncertainty of prediction of salt-water intrusion.

5.1 Acknowledgment

The support of the US Agency for International Development (AID) is acknowledged with gratitude.

5.2 References

Bear J., 1979, *Hydraulics of Groundwater.* Mac Graw Hill, 567 pp.

Bear J. and G. Dagan, 1964a. Some exact solutions of interface problems by means of the hodograph method, J. Geophys. Res., 69, 1563-1572.

Bear J. and G. Dagan, 1964b, Moving interface in coastal aquifers, J. Hydraul. Div. Am. Soc. Civ. Eng., 90, 193-216..

Dagan G. and J. Bear, 1968. Solving the problem of interface upconing in a coastal aquifer by the method of small perturbations. J. Hydraul. Res., 6, 15-44.

Dagan G., *Flow and Transport in Porous Formations,* 1989. Springer, pp. 465.

Henry H.R, 1959. Salt intrusion into freswater aquifers, J. Geophys. Res., 64, 1911-1919.

Huyarkon P.S., Andersen P.F., Mercer J.W. and White H.O., 1987. Salt intrusion in aquifers: development and testing of a three dimensional finite element model. Water Resources Research, 23, 293-319.

22

Keulegan H.D., 1954. An example report on model laws for density currents, National Bureau of Standards Report, Dept. of Commer., Washington D.C.

Liu, P.L.-F., Cheng, A.H.-D., Liggett, J.A. and Lee, J.H., Boundary integral equation solutions of moving interface between two fluids in porous media. Water Resour. Res., 17, 1445-1452, 1981.

Mercer J.W., Larson, S.P. and Faust, C.R., 1980. Simulation of salt water interface motion, Ground Water 18, 374-385

Mualem Y. and Bear J.,1974. The shape of the interface in steady flow in a stratified aquifer. Water Resour. Res., 10, 1207-1215.

Rumer R.R. and Shiau J.C., 1968. Salt water interface in a layered coastal aquifer, Water Resour. Res., 4, 1235-1247.

Segol G. and Pinder G.F., 1976. Transient simulation of salt water intrusion in south eastern Florida, Water Resources Research, Vol. 12, 65-70.

Shamir U. and Dagan G., 1971. Motion of the Seawater Interface in Coastal Aquifers: A numerical Solution. Water Resources Research, 7, 644-657.

Taigbenu, A.E., Liggett, J.A. and Cheng, A.H.D., Boundary integral solution to seawater intrusion in coastal aquifers. Water Resour. Res., 20, 1150-1158, 1984.

Wilson, J.L., and Sa da Costa, A., Finite element simulation of a saltwater/freshwater interface with indirect toe tracking. Water Resour. Res., 20, 1150-1158, 1982.

5.3 Appendix 1: General solution of (33)

The two equations appearing in (33) may be written as follows

$$(1-\eta^2)\frac{df}{d\eta} - 2\int_{-1}^{\eta} f(\eta')\,d\eta' = -E(\eta) \qquad \text{(A1.1)}$$

where $f(\eta)$ represents the functions $f_1(\eta)$ or $f_2(\eta)$, $E(\eta)$ represents the forcing terms for both equations and $\eta = (2/D)(z - D/2)$. After differentiation of (A1.1), the following equation is obtained

$$\frac{d}{d\eta}[(1-\eta^2)\frac{df}{d\eta}] - 2f = -\frac{\partial E(\eta)}{\partial \eta} \quad (-1 \le \eta \le 1\,) \qquad \text{(A1.2)}$$

The functions $E(\eta)$ are different for the equations in f_1 and f_2. For the first equation $E(\eta) = C_1(\eta)$ and for the second equation $E(\eta) = -E_2(\eta)$

23

(33).

In order to derive the solution of equation (A1.2), we introduce the Green function $G(\eta, r)$, solution of the following equation.

$$\frac{d}{d\eta}[(1-\eta^2)\frac{dG}{d\eta}] - 2G = \delta(\eta - r) \quad (-1 \leq \eta \leq 1) \qquad \text{(A1.3)}$$

where the function δ denotes the Dirac function. The solution of equation (A1.3) may be written in terms of the Green function as follows:

$$f(\eta) = -\int_{-1}^{+1} G(\eta, r)\frac{\partial E(r)}{\partial r}dr \quad (-1 \leq \eta \leq 1) \qquad \text{(A1.4)}$$

The eigenfunctions of the differential operator appearing in the basic equation (A1.3) are the Legendre polynomials $P_n(\eta)$. Thess polynomials form an orthogonal basis of the space of integrable functions defined in the interval $[-1, 1]$. Three important properties used in the following are summarized here: (a) $|P_n(\eta)| \leq 1$; (b) $\int_{-1}^{+1} P_m(\eta)P_n(\eta)d\eta = \left\{ {2/(2m+1) \quad if\ m=n \atop 0 \quad if\ m \neq n} \right\}$; (c) if $R(\eta)$ is a polynomial of degree $k < n$ then $\int_{-1}^{+1} P_n(\eta)R(\eta)d\eta = 0$.

The eigenvalues associated with the differential operator of equation (A1.3) are given by $\lambda_n = -(n^2 + n + 2)$.]

We consider a series expansion of the Green function $G(\eta, r) = \sum_{k=0}^{\infty} a_n(r)P_n(\eta)$. Using the orthogonality property (b) and after integration of equation (A1.2) over the interval $[-1, 1]$,one can show that $a_n(r) = -b_n P_n(r)$, where $b_k = (2n+1)/(n^2+n+2)$.

The solution of equation (A1.2) may be written in terms of the Green function as follows

$$f(\eta) = \sum_{n=0}^{\infty} \frac{2n+1}{n^2+n+2} P_n(\eta) \int_{-1}^{+1} P_n(r)\frac{\partial E(r)}{\partial r}dr \quad (-1 \leq \eta \leq 1) \qquad \text{(A1.5)}$$

We expand the solution $f(z)$ in a perturbation series $f(z) = f_0(z) + f_1(z) + f_2(z) + O(\sigma^3)$. The formula for the average field $< f(z) >$ and the variance $\sigma_f^2(z)$ are given by

$$< f(z) >= f_0(z) + < f_2(z) >= f_0(z) - \int_{-1}^{+1} G(\eta, r)\frac{\partial \langle E_2(r) \rangle}{\partial r}dr \qquad \text{(A1.6)}$$

$$\sigma_f^2(z) = < (f_1(z))^2 >= \int_{-1}^{+1}\int_{-1}^{+1} G(\eta, r_1)G(\eta, r_2)\frac{\partial^2 \langle C_1(r_1, r_2) \rangle}{\partial r_1 \partial r_2}dr_1 dr_2$$

24

It can be shown that at first-order in I', integration in (A1.6) leads to polynomials of degree two (See Appendix 2). Using properties (c) of the Legendre polynomials, the Green function reduces to a polynom of second degre and the same results as in Appendix 2 may be deduced.

5.4 Appendix 2: Derivation of $C_{11}(\eta_1, \eta_2)$ and $\langle E_2 \rangle$.

The random function $C_1(\eta)$, of zero mean, is defined by Eq. (30). The covariance $C_{11}(\eta_1, \eta_2) = \langle C_1(\eta_1)\, C_1(\eta_2) \rangle$ has the following exact expression

where $A(a,b,c,d) = (1/4\sigma^2 I) \int_a^b \int_c^d C_{\mathcal{K}}(u,v)\, du\, dv$. Under the approximation $C_{\mathcal{K}}(u,v) = 4\sigma^2 I\, \delta(u-v)$

$$\begin{aligned} C_{11} \;=\; & 4\sigma^2 I[(1+\eta_1)(1+\eta_2)\, A(\eta_1,1,\eta_2,1) + (1+\eta_1)(1-\eta_2)\, A(\eta_1,1,-1,\eta_2) + \\ & (1-\eta_1)(1+\eta_2)\, A(-1,\eta_1,\eta_2,1) + (1-\eta_1)(1-\eta_2)\, A(-1,\eta_1,-1,\eta_2) - \\ & \frac{1}{2}(1+\eta_1)(1-\eta_2^2)\, A(\eta_1,1,-1,1) - \frac{1}{2}(1-\eta_1)(1-\eta_2^2)\, A(-1,\eta_1,-1,1) - \\ & \frac{1}{2}(1-\eta_1^2)(1+\eta_2)\, A(\eta_2,1,-1,1) - \frac{1}{2}(1-\eta_2)(1-\eta_1^2)\, A(-1,\eta_2,1,-1,1) + \\ & \frac{1}{2}(1-\eta_1^2)(1-\eta_2^2)\, A(-1,1,-1,1)] \end{aligned} \tag{A2.1}$$

we have for $\eta_1 \geq \eta_2$

$$\begin{aligned} A(\eta_1,1,\eta_2,1) &= 1-\eta_1\ ;\ A(\eta_1,1,-1,\eta_2) = 0\ ;\ A(-1,\eta_1,\eta_2,1) = \eta_1 - \eta_2\ ; \\ A(-1,\eta_1,-1,\eta_2) &= 1+\eta_2\ ;\ A(\eta_1,1,-1,1) = 1-\eta_1\ ; \\ A(-1,\eta_1,-1,1) &= 1+\eta_1\ ;\ A(\eta_2,1,-1,1) = 1-\eta_2\ ;\ A(-1,\eta_2,1,-1,1) = 1+\eta_2\ ; \\ A(-1,1,-1,1) &= 2 \end{aligned} \tag{A2.2}$$

Substitution of (A2.2) into (A2.1) leads to the result C_{11} (36). Next, we evaluate $\langle C_2(\eta) \rangle$ (30). The exact expression is

$$\langle C_2 \rangle = 4\sigma^2 I[A(-1,\eta,\eta,1) - \frac{1}{2}(1+\eta)A(\eta,1,-1,1) - \frac{1}{2}(1-\eta)A(\eta,1,-1,1) + \frac{1}{4}(1-\eta^2)A(-1,1,-1,1)] \tag{A2.3}$$

By the same approximation as in (A2.2) we get for $\langle C_2 \rangle$ the result of (39). The expression (39) of $\langle F_2(\eta)\, d^2F_2(\eta)/d\eta^2 \rangle = \lim_{\eta_1 \to \eta, \eta_2 \to \eta} \partial^2 C_F(\eta_1,\eta_2)/\partial\eta_1^2$ is obtained by differentiation in (37), leading to the final result (39) for $\langle E_2 \rangle$.

25

5.5 Figure captions

Fig. 1 Definition sketch of an interface in steady flow.

Fig. 2 The mean interface profile $\langle\chi'\rangle$ (Eq. 17) and the intervals of confidence $\pm 2\,\sigma_\chi$ (Eq. 21) for $\sigma_Y = 1$, $I' = I/D = 0.01$, $Q/K"D = 1/6$.

Fig. 3 Definition sketch for a coastal collector withdrawaling fresh water above the interface.

Fig. 4 The dependence of the fresh water discharge to the sea Q'_s and its interval of confidence $\pm 2\,\sigma_{Q_s}$ (Eq. 24) on the elevation of the upconned interface ζ'_d beneath the coastal collector at x'_d ($\sigma_Y = 1$, $I' = I/D = 0.01$, $Q/K"D = 1/6$).

Fig. 5 The mean interface profile $\langle\chi'^c(\zeta'|\zeta'_1)\rangle$ and its interval of confidence (Eq. 26), conditioned on a measurement $\zeta'_1 = 0.4$ at $x'_1 = 1$ ($\sigma_Y = 1$, $I' = I/D = 0.01$, $Q/K"D = 1/6$).

Fig. 6 The reduction of the variance of the toe coordinate $\sigma_\chi^{c,2}(D|\zeta_1)/\sigma_\chi^2(D)$ (Eq. 26) as function of the measured interface depth ζ'_1 ($\sigma_Y = 1$, $I' = I/D = 0.01$, $Q/K"D = 1/6$).

Fig. 7 Definition sketch for the Keulegan solution (dashed line, Eq. 32) and its generalization for a layered aquifer (full line).

26

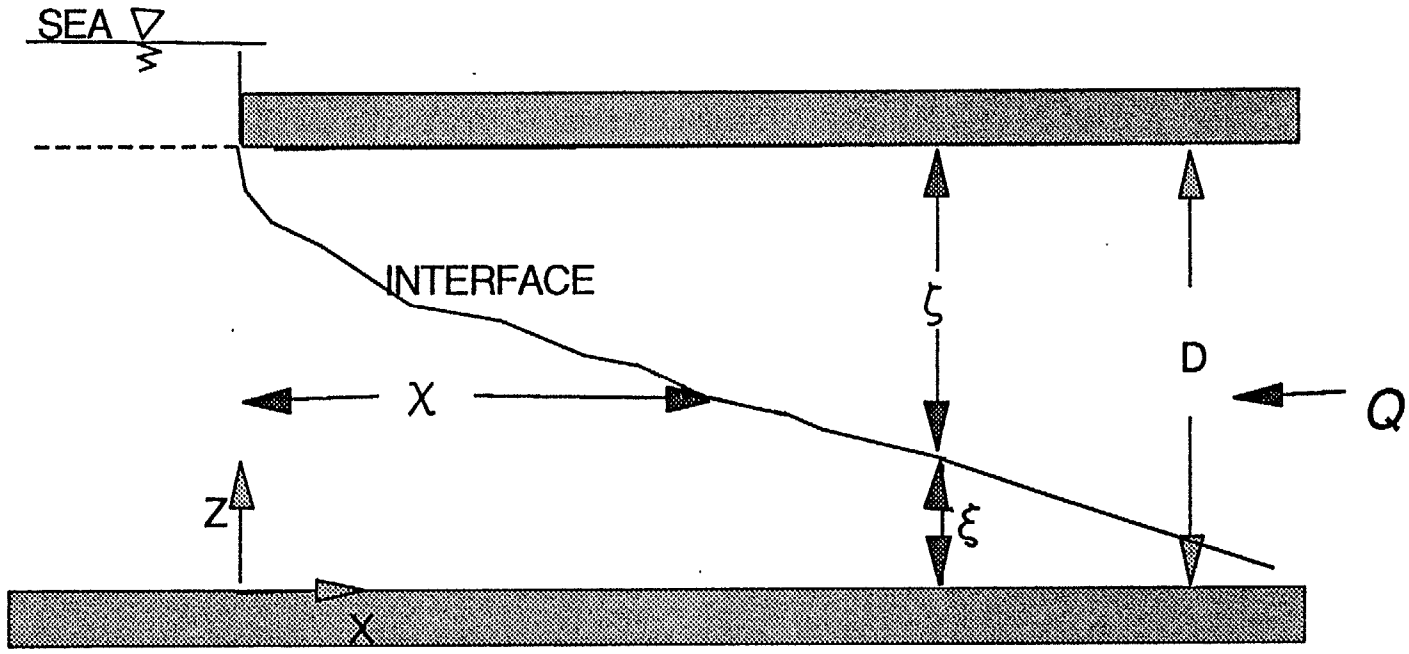

Fig. 1

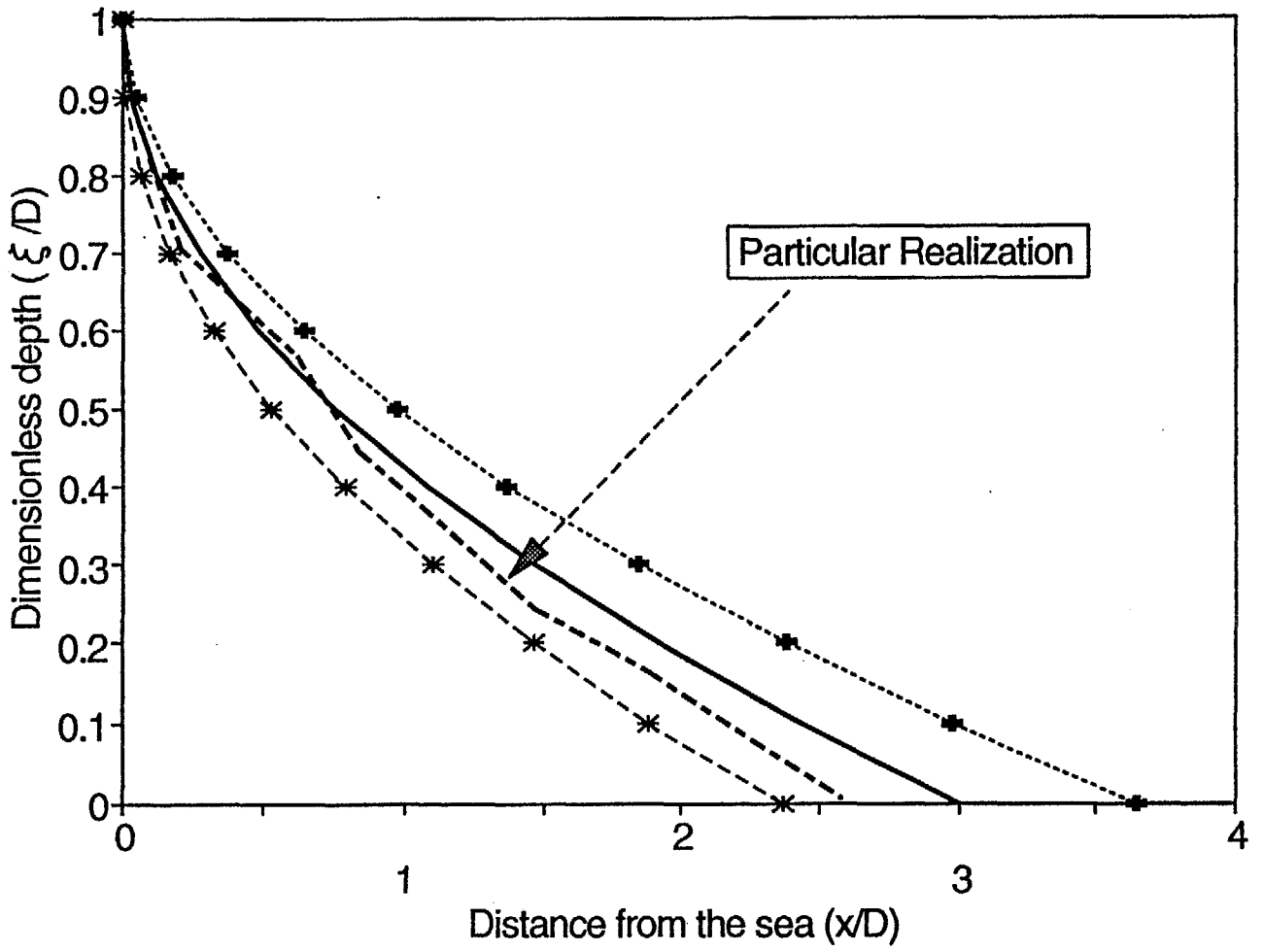
Particular Realization
Dimensionless depth (ξ /D)
Distance from the sea (x/D)
0
0.1
0.2
0.3
0.4
0.5
0.6
0.7
0.8
0.9
1
0
1
2
3
4

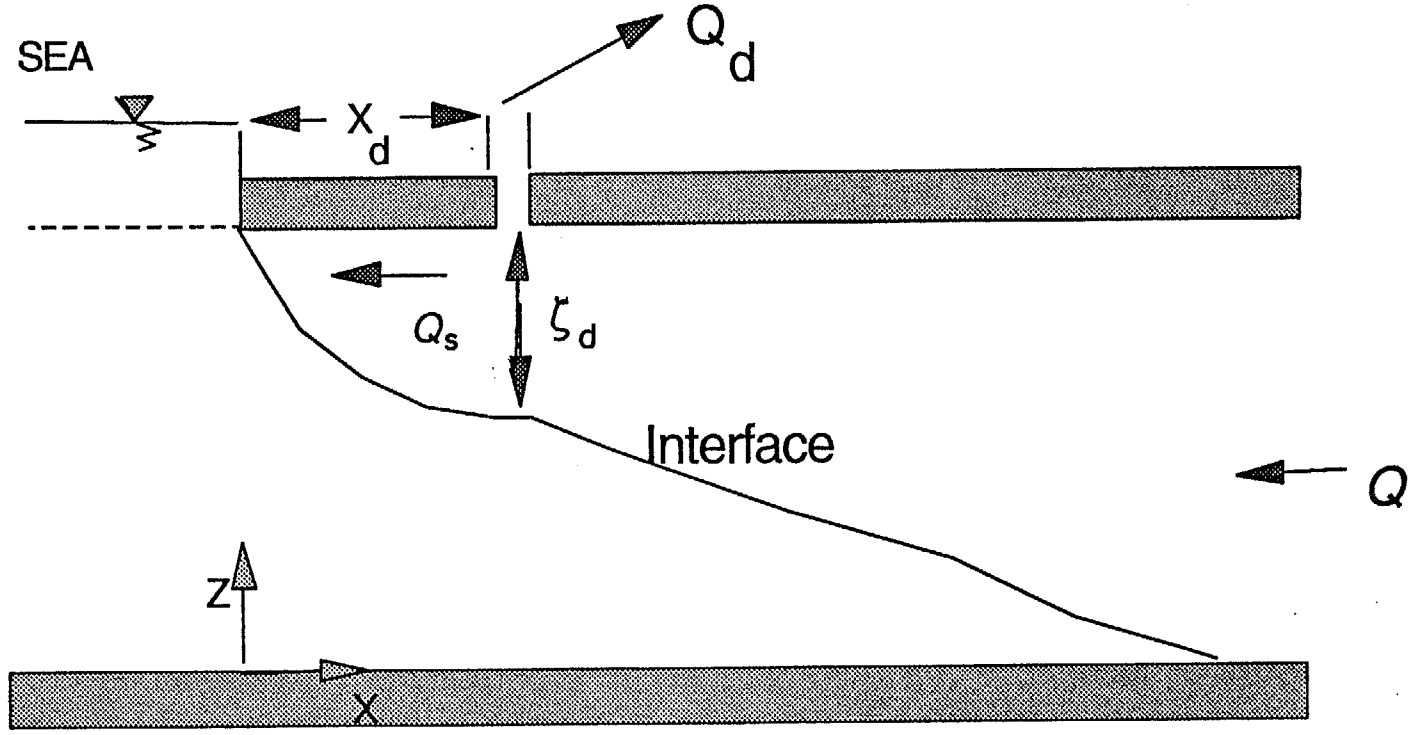
SEA
Q_d
X_d
Q_s
ζ_d
Interface
Q
Z
X

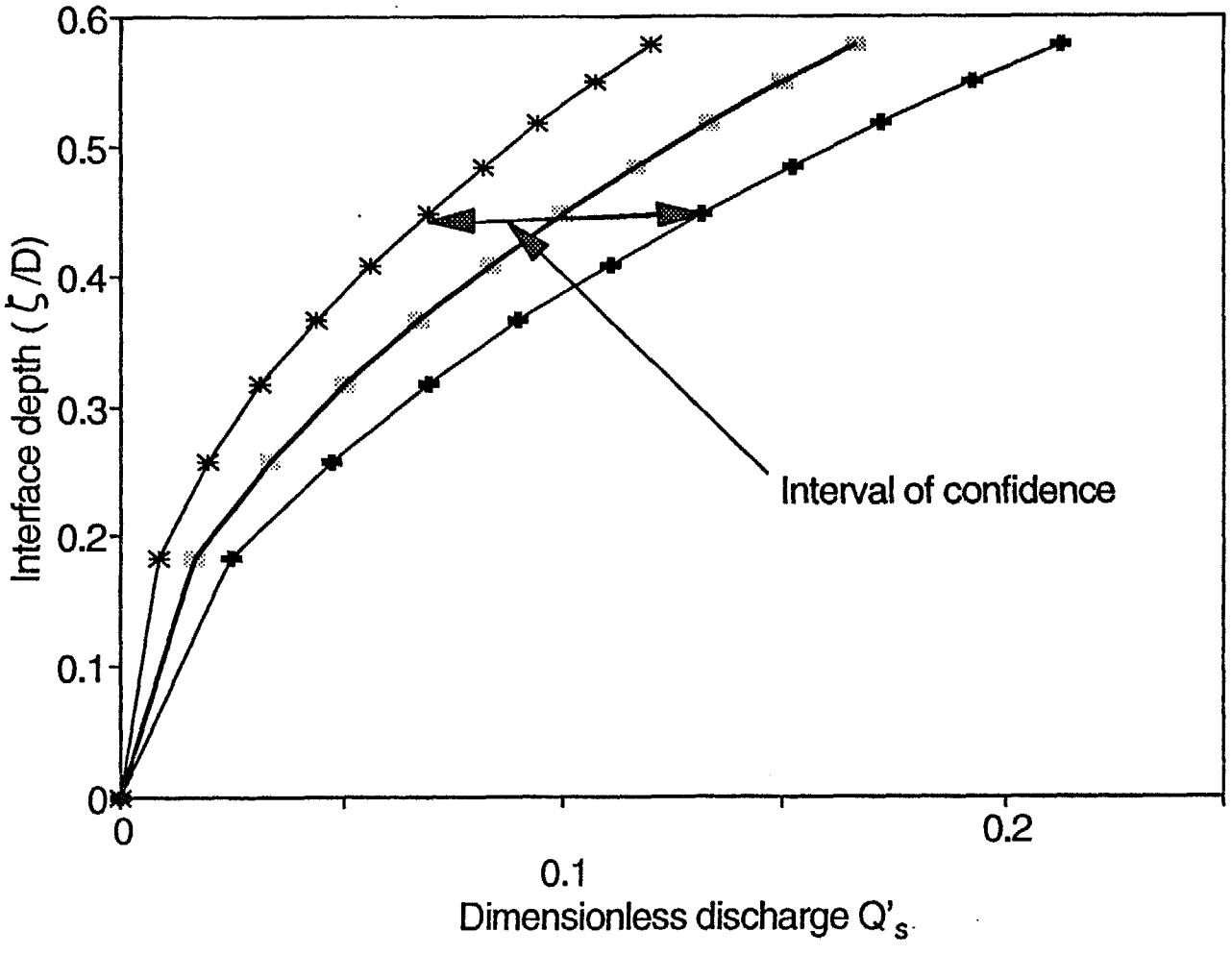
0.6
0.5
0.4
0.3
0.2
0.1
0
Interface depth (ζ /D)
0
0.1
0.2
Dimensionless discharge Q's
Interval of confidence

Fig. 4

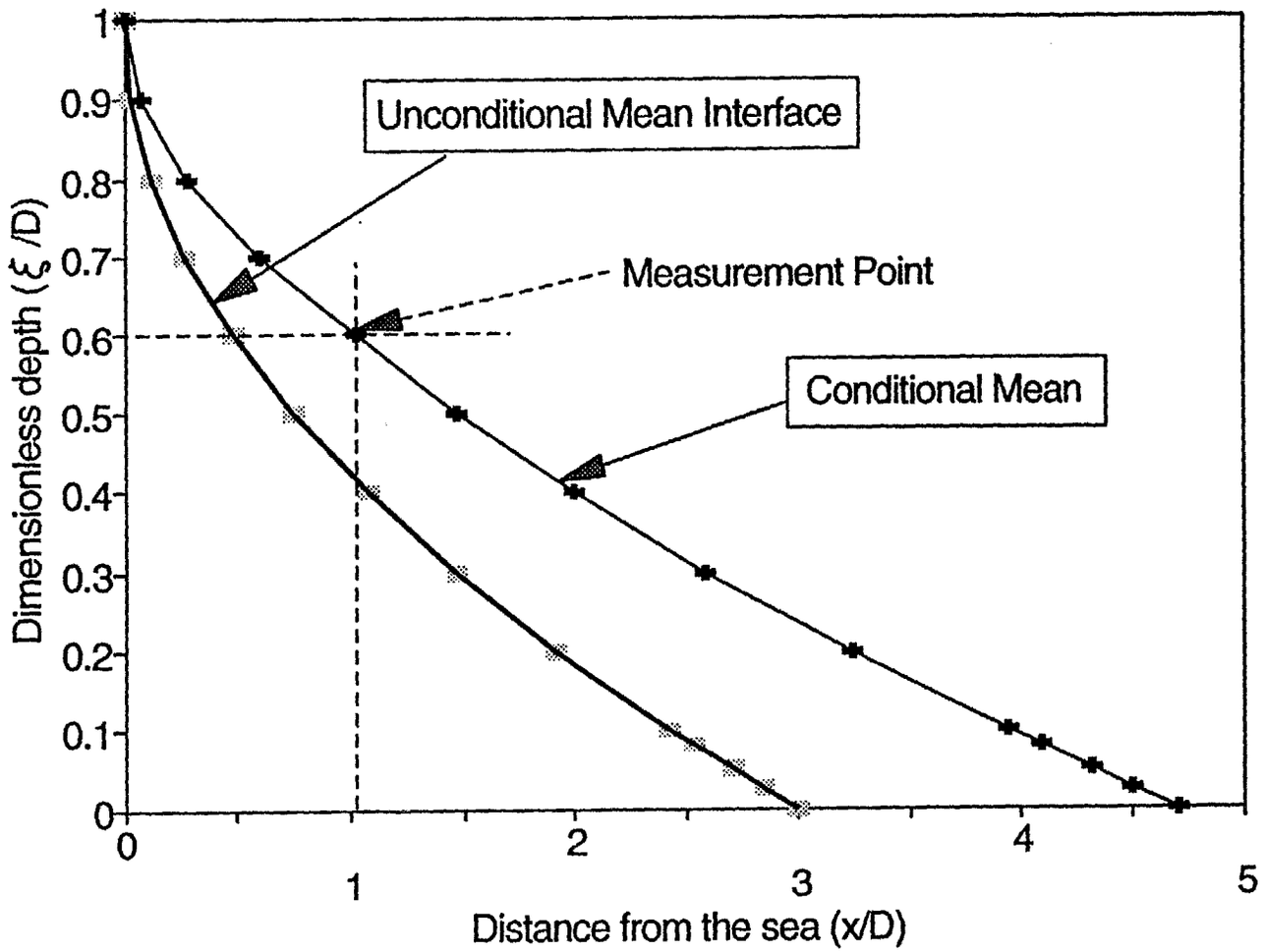
Unconditional Mean Interface
Measurement Point
Conditional Mean
Dimensionless depth (ξ /D)
Distance from the sea (x/D)
0
0.1
0.2
0.3
0.4
0.5
0.6
0.7
0.8
0.9
1
0
1
2
3
4
5

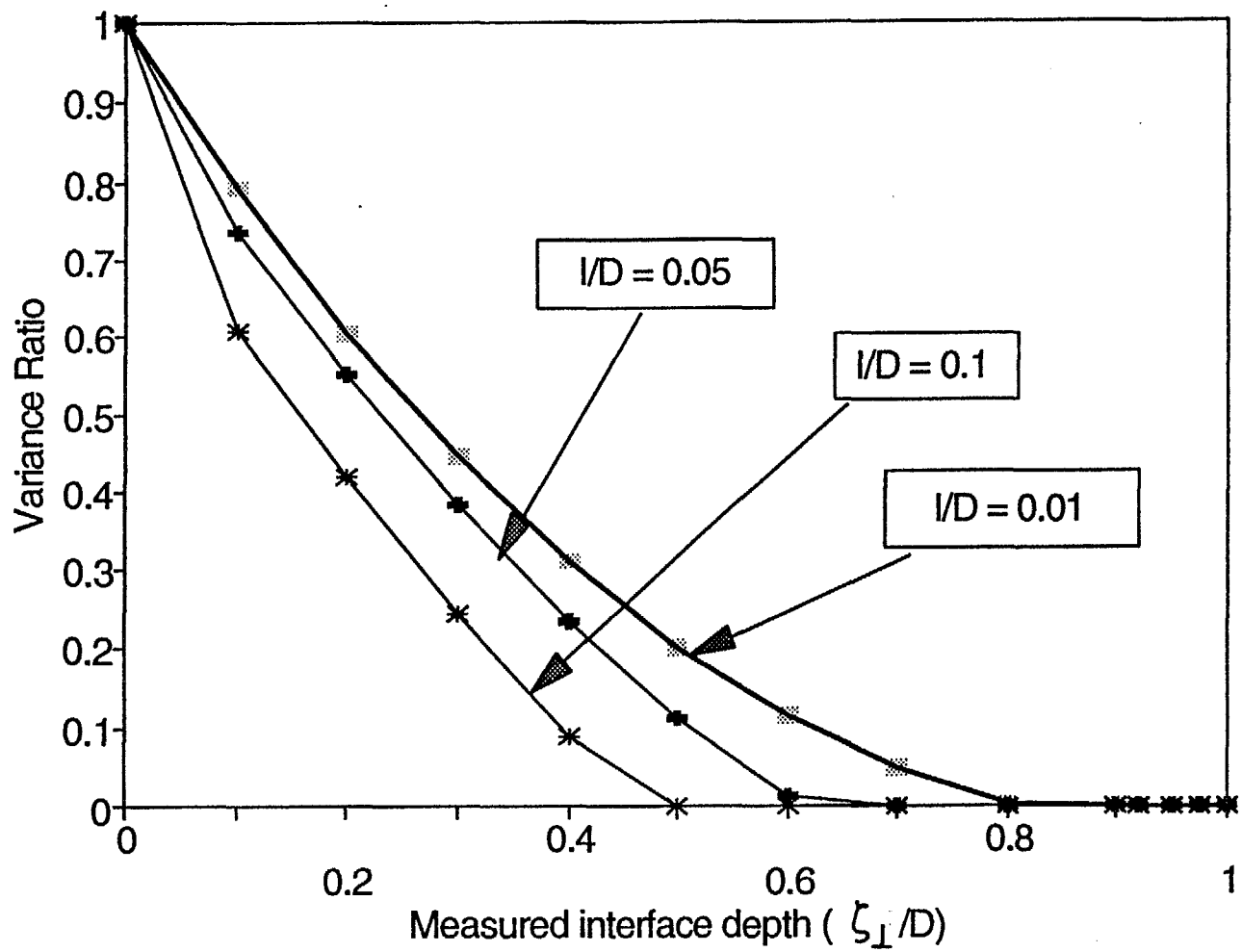
Variance Ratio
1
0.9
0.8
0.7
0.6
0.5
0.4
0.3
0.2
0.1
0
0
0.2
0.4
0.6
0.8
1
Measured interface depth ($\zeta_\perp$ /D)
l/D = 0.05
l/D = 0.1
l/D = 0.01

Fig. 6

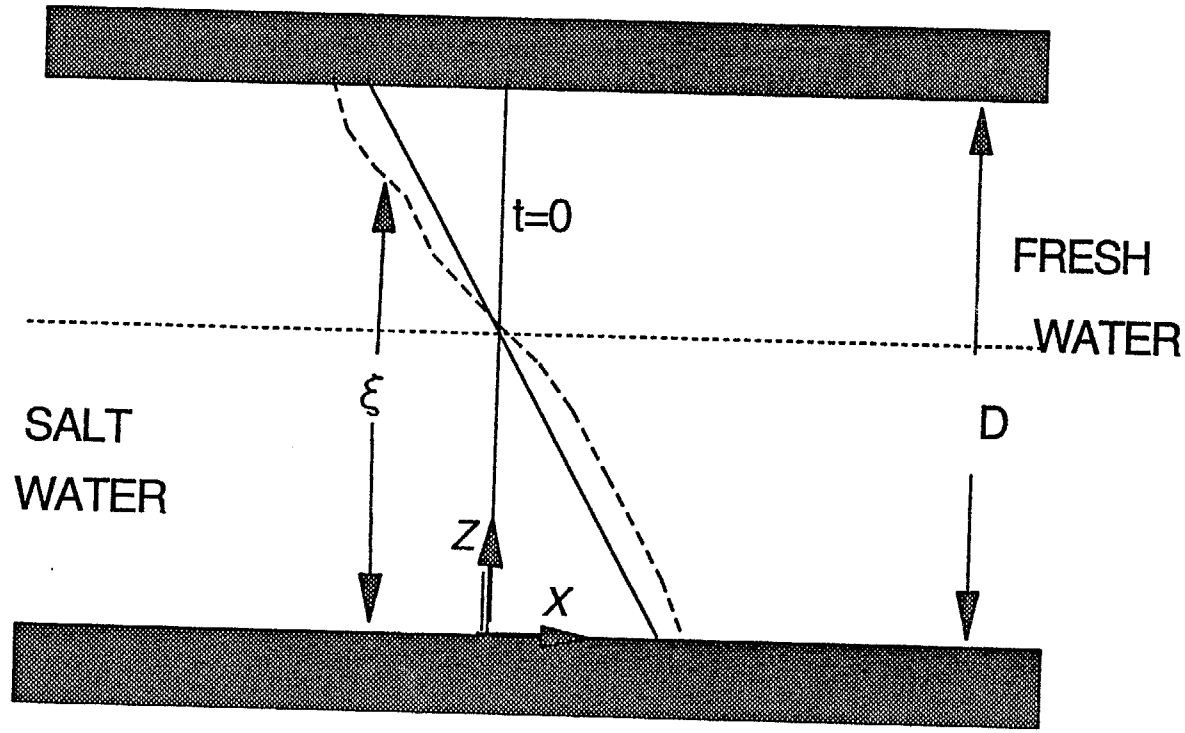

Fig. 7

Locating Salt/Fresh Water Interface Using Nonlinear Programming and H-Adaptive BEM*

A. Naji† D. Ouazar‡ A. H-D. Cheng§

Abstract

The location of sharp interface between salt and freshwater in coastal aquifer is determined using optimization techniques. The algorithm is based on the combination of a nonlinear programming and an h-adaptive boundary element method. The objective is to create to an automated solution procedure. The effectiveness of the model is demonstrated using several examples in confined and unconfined aquifers. The unconfined aquifer cases require the simultaneous determination of an interface and a free surface.

1 Introduction

Coastal aquifers are prone to the encroachment of saltwater from the sea. Saltwater with a higher density tends to flow underneath a static freshwater and invades inland. Normally there exists a freshwater outflow that counters the saltwater intrusion such that steady-state interface can be maintained. However, anthropogenic activities in coastal zones have led to aquifer over-exploitation. The historical balance of salt-fresh water interface may be upset, causing a lost of freshwater resources.

To combat saltwater intrusion, water resources managers need to determine the location of salt/fresh water interface under various hydrological and human water consumption conditions. The simulation is normally carried out by numerical modeling using methods such as finite element, finite difference and boundary element. In the present work, the boundary element method (BEM) is adopted. The BEM is well known for its ability to

*Submitted to Computers and Structures. Last revised March 13, 1996.

†Université Abdelmalek Essaadi, Faculté des Sciences et Techniques, B.P. 416, Tanger, Morocco.

‡Université Mohammed V, Ecole Mohammadia d'Ingénieurs, LASH, B.P. 765, Agdal, Rabat, Morocco.

§Department of Civil and Environmental Engineering, University of Delaware, Newark, Delaware 19716, USA.

34

reduce the dimensionality of solution mesh. This trait is particularly useful in handling moving boundaries that are encountered in saltwater intrusion problems.

Applying BEM to locate steady-state seepage free surface was pioneered by Liggett [1]. The technique involves simulating transient flow until it reaches steady state. For locating free surface in open channel flow, the first application of BEM was presented by Cheng, *et al.*[2] using a rudimentary gradient search method. For saltwater intrusion applications, the transient approach was taken by Liu, *et al.*[3] and Taigbenu, *et al.* [4] to track down the steady interface. In the present paper, the steady-state sharp interface is located utilizing optimization techniques. The process used is based on the combination of nonlinear programming and an h-adaptive BEM.

The h-adaptive boundary element method has been successfully applied to flow problems, such as cavity, sluice gate, spillway and earth dam flows [5, 6, 7], as well as many other problems [8, 9, 10, 11]. The basic idea is to generate an optimal discretization of a considered saltwater intrusion problem automatically. In such an optimal mesh both the problem geometry and the function variation are properly represented. The solution obtained, which depends on the mesh used, is more accurate. The h-adaptive algorithm used in this paper is based on the calculation of the residual function deduced from the boundary integral equation, to define the predicted errors. Starting from an initial coarse mesh, the process is applied to refine the mesh locally, if necessary, by subdividing existing elements. The global predicted error computed throughout iterations provides information about the global accuracy of the solution and guides the process until convergence.

The mathematical problem of locating unknown surfaces is formulated as an optimization problem. The objective functions, which are nonlinear, are constructed based on the redundant boundary condition given on the unknown surfaces. The interface of phreatic surface nodes are considered as design variables. Constraints are applied to limit the region of search to avoid possible inconsistent trial geometries. The nonlinear programming is used to guide the trial and error process to determine the interface and phreatic surface locations. The h-adaptive BEM is used to solve the direct boundary value problem at each trial stage.

The objective of the work is to generate an automated solution procedure to solve sharp interface saltwater intrusion problems. The effectiveness of the algorithm is evaluated by a number of confined and unconfined aquifer problems.

35

2 Problem Formulation

Two approaches can be used to model saltwater intrusion problems. One is based on hydrodynamics dispersion and the other on sharp interface. The first approach is considered when the mixing zone between salt and fresh water cannot be neglected. The second technique is adopted when the thickness of the transition zone is much smaller than the aquifer dimension. In this case, the flow region is divided into two zones separated by a sharp interface whose location is to be determined. Only the sharp interface approach will be considered in this paper.

The problems solved here involve vertical, two-dimensional aquifer sections. In a homogeneous, isotropic aquifer, the governing equation is

$$\nabla^2 h = 0 \tag{1}$$

where h is the piezometric head of freshwater. It is assumed that the saltwater region is static, hence the saltwater head h_s is a constant. There are several types of boundary conditions. In particular, we note the following: on free surface,

$$h = y \tag{2}$$

and on the salt-freshwater interface

$$h = \frac{\rho_f - \rho_s}{\rho_f} y \tag{3}$$

where y is the elevation from datum, and ρ_f, ρ_s are respectively the freshwater and saltwater density. On these locations, a second boundary condition also exists:

$$\frac{\partial h}{\partial n} = 0 \tag{4}$$

On a fixed boundary, the second boundary condition is redundant and generally cannot be tolerated. On free surface and interface, however, their locations are not known *a priori*. The second condition is essential in the determination of their unique locations.

3 Optimization

Free surface and interface are characterized by the existence of two boundary conditions as previously indicated. One of these conditions can be used to transform the problem into an optimization one, with the free surface position nodes as the unknown design variables.

36

Consider a free boundary value problem $\mathcal{P}1$:

$$\mathcal{P}1 : \begin{cases} \nabla^2 h = 0 & \text{in} \quad \Omega \\ \mathcal{B}_1\, h = g_1 & \text{on} \quad \Gamma_1 \\ \mathcal{B}_2\, h = g_2 & \text{on} \quad \Gamma_2 \\ \mathcal{B}_3\, h = g_3 & \text{on} \quad \Gamma_2 \end{cases} \tag{5}$$

where Ω is a bounded domain under investigation, with the boundary $\Gamma = \Gamma_1 \cup \Gamma_2$, Γ_1 represents all fixed boundaries, and Γ_2 denotes the free boundaries (free surface and interface), $\mathcal{B}_i$ are various kinds of boundary operators, and g_i are smooth functions giving the boundary values. We note in particular that two boundary conditions are available on Γ_2.

A second problem is defined with a trial Γ_2 such that

$$\mathcal{P}2 : \begin{cases} \nabla^2 h = 0 & \text{in} \quad \Omega \\ \mathcal{B}_1\, h = g_1 & \text{on} \quad \Gamma_1 \\ \mathcal{B}_2\, h = g_2 & \text{on} \quad \Gamma_2 \end{cases} \tag{6}$$

An objective function f is constructed by minimizing the difference between the prescribed function g_3 in $\mathcal{P}1$ and the computed $\mathcal{B}_3\, h$ in $\mathcal{P}2$

$$f(\Gamma_2) = \|\mathcal{B}_3\, h - g_3\| \tag{7}$$

where $\|\|$ is a certain norm evaluated on Γ_2. f is computed each time the free boundary Γ_2 is moved.

The shape design problem is given by:

$$\mathcal{P}3 : \text{minimize} \;\; f(\Gamma_2) \text{ for } \Gamma_2 \in \Lambda \tag{8}$$

where Λ is a family of domains Ω within which one wishes to minimize f. The constraint is that each element Ω of the set Λ must have a physical meaning.

The solution of the problem $\mathcal{P}3$ is based on the following four main steps:

1. The location of the free boundary Γ_2 is either given (for the first iteration) or determined (for subsequent iterations).

2. The problem $\mathcal{P}2$ is solved by the BEM to compute h and its normal derivative.

3. The value of the objective function f is computed using (7).

4. The direction vector of minimization is determined.

37

Discretizing the boundary into N_e elements with N_f nodes on the free boundary, the continuum problem $\mathcal{P}3$ is transformed into a discrete one. It is given by the following:

$$\mathcal{P}4 : \begin{cases} \text{minimize} & \bar{f}(z_1, z_2, ..., z_{N_f}) \\ \text{subject to} & a_i \leq \psi_i(z_1, z_2, ..., z_{N_f}) \leq b_i \ \text{ for } \ i = 1, ..., N_f \end{cases} \tag{9}$$

where $(z_1, z_2, ..., z_{N_f})$ is a vector containing the position of the free boundary nodes, ψ_i are constraint functions generating the set Λ and prescribing bounds on the amplitude of the free boundary displacements, and $\bar{f}$ is the objective function to be minimized based on discrete values.

Although no analytical information about the behavior of the objective function (*i.e.* convexity, continuity, *etc.*) is available, it is assumed that the function is differentiable up to the second order. To avoid the use of penalty nonlinear programming techniques, the constrained minimization problem $\mathcal{P}4$ can be transformed into an unconstrained one by introducing all constraint functions ψ_i in a uni-dimensional search [7]. The problem becomes easier to solve.

The sensitivity of either potential or flux contained in the unknown vector $\boldsymbol{x}$ of the algebraic system $\boldsymbol{Ax} = \boldsymbol{B}$ is given by the application of a finite difference formula. The technique is formulated by solving two systems, one

$$\boldsymbol{A}(z_i)\boldsymbol{x}(z_i) = \boldsymbol{B}(z_i) \tag{10}$$

associated with design variables z_i and the other

$$\boldsymbol{A}(z_i + \delta z_i)\boldsymbol{x}(z_i + \delta z_i) = \boldsymbol{B}(z_i + \delta z_i) \tag{11}$$

related to perturbed design variables $z_i + \delta z_i$, in which δz_i are a small perturbations. The sensitivity of $\boldsymbol{x}$ with respect to z_i, denoted by $\partial \boldsymbol{x}/\partial z_i$, is determined using the following equation:

$$\frac{\partial \boldsymbol{x}}{\partial z_i} \simeq \frac{\boldsymbol{x}(z_i + \delta z_i) - \boldsymbol{x}(z_i)}{\delta z_i} \tag{12}$$

We note that the matrix $\boldsymbol{A}(z_i + \delta z_i)$ has to be computed for each design variable z_i and a large number of systems of equations have to be solved.

The objective functions for both confined and unconfined examples are based on minimizing the calculated flux at free boundaries. The boundary condition $q = \partial h/\partial n = 0$ is used to define the objective function,

$$f(z_1, ..., z_{N_f}) = \frac{1}{2}\sum_{i=1}^{N_f} q_i^2 \tag{13}$$

38

The parameters z_i are considered to be y_i coordinates for a phreatic surface (unconfined aquifer problem) and x_i coordinates for an interface (confined and unconfined aquifers). The nodes are adjusted vertically and horizontally, respectively.

The only constraint associated to the minimization problem is imposed on the parameters z_i, in order to limit the region to a physically acceptable geometry. The constraint can be expressed through inequalities in the form:

$$z_{\min} \leq z_i \leq z_{\max} \; \forall \, i \in \{1, ..., N_{\mathrm{f}}\} \tag{14}$$

The values of $z_{\min}$ and $z_{\max}$ depend on the problem on hand.

To search for the direction of minimization, the Gauss Marquardt algorithm is used. If $\boldsymbol{z}^k$ is the free surface location at iteration k, the new position is given by the linear equation

$$\boldsymbol{z}^{k+1} = \boldsymbol{z}^k + \alpha \boldsymbol{\delta}^k \tag{15}$$

in which $\boldsymbol{\delta}^k$ is the vector of the search direction at iteration k, and α is a step length for the movement along the search direction, determined by the one dimensional minimization problem. Vector $\boldsymbol{\delta}^k$ is given by

$$\boldsymbol{\delta}^k = -\boldsymbol{H}^k \Delta \boldsymbol{f}^k \tag{16}$$

where $\boldsymbol{H}$ is the Hessian matrix approximated by

$$\boldsymbol{H} = (\boldsymbol{J}^{\mathrm{T}} \boldsymbol{J} + \lambda \boldsymbol{I})^{-1} \tag{17}$$

$\boldsymbol{J}$ is the Jacobian matrix obtained by a finite difference procedure, $\boldsymbol{I}$ is the identity matrix, and λ is a given constant which decreases with increasing iterations.

The constrained optimization problem can be transformed into an unconstrained one by introducing constraints in a uni-dimensional search. To achieve this, an $\alpha_{\max}$ should be found such that all new nodal positions satisfy the constraints (*i.e.* still in the feasible domain). The optimal α must be determined using an uni-dimensional search in the domain $[0, \alpha_{\max}]$. The Fiboccanoi's method is used to find such an optimum.

4 H-Adaptive BEM

Discretization is one of the most important factors in numerical modeling of a boundary value problem since the approximate solution largely depends on the number and the order of elements used. A rigorous definition of an optimal mesh is the one for which the error of the numerical solution is reduced to a minimum, and is uniformly distributed over the elements of the mesh. To obtain such an optimal mesh, a mesh redesign procedure

39

is necessary for controlling the refinement process and calculating an accurate solution. In recent years, attention has been drawn to use error estimates in the BEM to guide a refinement strategy.

Error estimators can be divided into two categories: *a-priori* error estimators requiring the knowledge of either the exact solution or the behavior of the approximate one; and *a-posteriori* error estimators, which extract guidelines from a prediction of the exact solution, based on the approximate one.

The computation of error estimators is based on an appropriate norm providing a measure of the difference between the numerical solution $\bar{h}$ associated to a given mesh, and the exact or predicted solution h of the problem. As has been demonstrated based on some regularity of the boundary conditions, the solution of the BVP belongs to the Sobolev space H^k ($k = 1$ or 2) and its associated norm can be used to measure the error.

The norms L^2 and H^1 have been extensively used to estimate the value of error in boundary element analyses. They are defined as follows:

$$\int_\Gamma (h - \bar{h})^2 \; d\Gamma \quad \text{for } L^2 \text{ norm} \tag{18}$$

$$\int_\Gamma \left[(h - \bar{h})^2 + (h' - \bar{h}')^2\right] \; d\Gamma \quad \text{for } H^1 \text{ norm} \tag{19}$$

in which h and $\bar{h}$ are the exact (or predicted) and approximate solutions, respectively, h' and $\bar{h}'$ are their tangential derivatives. Error estimates in the BEM are measured by integration over the boundary only. The popularity of these two norms may be explained by their simplicity as compared to other norms like H^k for $k \geq 2$, for which higher-order derivatives are needed.

Problems considered in this paper are governed by Laplace or Poisson equations subject to appropriate boundary conditions. The boundary integral equation is given by:

$$c(\boldsymbol{x})h(\boldsymbol{x}) + \int_\Gamma h(\boldsymbol{x}')q^*(\boldsymbol{x}', \boldsymbol{x}) \, d\boldsymbol{x}' = \int_\Gamma h^*(\boldsymbol{x}', \boldsymbol{x})q(\boldsymbol{x}') \, d\boldsymbol{x}' + \int_\Omega b(\boldsymbol{x}')u^*(\boldsymbol{x}', \boldsymbol{x}) \, d\boldsymbol{x}' \tag{20}$$

where h^* is the fundamental solution of Laplace equation, q stands for normal derivative, $\boldsymbol{x}$ and $\boldsymbol{x}'$ are the source and field points, and c is a Cauchy principal value coefficient. Equation 20 is satisfied at all nodal (collocation) points, but its application to other boundary points produces an error or a residual.

Theoretical studies have shown that the residual function can be taken as an approximation or estimation of the exact error. Integrating the square of the residual over the boundary defines the error estimator, and over each element defines the error indicators. These two errors provide an accurate and reliable mechanism for automatic redesign of a mesh, and have been developed by various authors [8, 9, 10, 11] in the context of boundary

40

element method. They are given by the following two equations:

$$\nu^2 = \|r\|_{L^2}^2 = \int_\Gamma r^2 \, dx' = \sum_{e=1}^{N_e} \lambda_e^2 \tag{21}$$

$$\lambda_e^2 = \int_{\Gamma_e} r^2 \, dx' \tag{22}$$

where ν is the error estimator and λ_e is the error indicator in element e.

The error estimator is computed at each iteration to provide information on overall accuracy, and to stop mesh refinement if a specified tolerance is achieved. If the solution is considered not acceptable, refinement on each element will be controlled by error indicators which will decide where additional local refinement is required. The computation of the posterior error (local or global) requires evaluation of the residual along the boundary. Attention must be paid to this process since inaccuracy may lead to unnecessary refinement.

The philosophy behind adaptive refinement is to determine an optimal mesh, based on the minimization of the error up to an acceptable number of degrees of freedom, yet less than a specific number of nodes. The objective is to decide where the mesh should be refined and when this refinement should be stopped based on some error criteria. The prediction of more accurate solutions, starting from any initial mesh, can thus be achieved without any effort from the design engineer.

In the h-adaptive strategy, refinement is performed by increasing the number of elements through subdivision of those displaying large local errors at each iteration. Although some specified tolerance is used to verify convergence, other restrictions should be used to control the maximum number of nodes and the ratio between the size of neighboring elements. The basic algorithm of h-adaptive schemes consists of the following steps [11]:

- Step 1 : Choose a basic mesh, sufficient to describe the geometry and boundary conditions of the problem.
- Step 2 : Solve (20) subject to boundary conditions.
- Step 3 : Compute the error estimator and indicators. If the accuracy obtained by the error estimator is sufficient, stop.
- Step 4 : For each element, decide whether the accuracy measured by error indicators has to be improved. If yes, subdivide the element into two subelements. Return to step 2.

41

Consider the saltwater intrusion problem. Starting with an initial mesh, the h-adaptive algorithm is applied with a lower accuracy requirement until an optimal mesh for the current iteration is obtained. The free-surface location is then adjusted following the nonlinear programming search direction. The adaptivity scheme is introduced at every iteration of the free surface adjustment with increasing accuracy requirements, until the program is terminated by a nonlinear programming tolerance criterion.

5 Numerical Results

Several problems involving confined and unconfined aquifer geometries are investigated. In the first two problems, only the nonlinear programming part for adjusting free surface and interface geometries is examined. The combination of nonlinear programming with h-adaptive BEM is implemented for the remaining problems.

The first example tested is a confined aquifer problem, shown in Figure 1. The boundary conditions are:

$$\begin{aligned} h &= 0 && \text{on AB} \\ \frac{\partial h}{\partial n} &= 0 && \text{on BC, DE and EA} \\ \frac{\partial h}{\partial n} &= \frac{Q}{Kb} && \text{on CD} \\ h &= \frac{\rho_f - \rho_s}{\rho_f} y && \text{on EA} \end{aligned} \tag{23}$$

The following values are used: aquifer thickness $b = 27$ m, hydraulic conductivity $K = 69$ m/day, density of freshwater $\rho_f = 1$ g/cm^3, that of saltwater $\rho_s = 1.025$ g/cm^3, and the freshwater outflow rate (per unit width normal to the plane of flow) $Q = 18.8$ m^2/day. The boundary of the domain is discretized into 45 linear elements with 10 on the interface AE. With an initial trial interface as a straight line, the objective function value decreases from the initial value of 3.57×10^{-3} to the final value 5.7×10^{-7}. The average value of flux along the interface is around 10^{-4} m/day when the solution is accepted. The final interface location is presented in Figure 2. In the same figure, an analytical solution by Glover [12] is presented for comparison. The Glover solution represents the case of an infinite aquifer thickness, $b \to \infty$. The comparison is nevertheless quite good.

The next example involves an phreatic aquifer as shown in Figure 3. The conditions on various parts of boundary are

$$\begin{aligned} h &= y && \text{on AB and BC} \\ \frac{\partial h}{\partial n} &= 0 && \text{on AB and DE} \end{aligned}$$

- 42

$$
\begin{aligned}
\frac{\partial h}{\partial n} &= \frac{Q}{Kb} \qquad \text{on EA} \\
h &= \frac{\rho_f - \rho_s}{\rho_f} y \quad \text{on CD and DE}
\end{aligned} \tag{24}
$$

The parameters used are: $\rho_s/\rho_f = 1.08$, $Q/Kb = 0.0545$, and the angles $\alpha = 90°$, $\beta = 90°$. It is noted that these combination of parameters are sufficient to define the problem as shown in (24). The initial free surface and interface are plotted as dashed lines in Figure 4. The final converged surfaces are presented in solid lines in the same figure. The objective function associated with the phreatic surface decreases from 1.03×10^{-2} to 3.44×10^{-5} and the one of the interface changes from 3.98×10^{-2} to 1.11×10^{-5}. The average flux on the free boundaries is around 10^{-4}.

Two more saltwater intrusion problems are solved with the h-adaptive scheme combined with the optimization technique. The third problem is adopted from Detournay and Strack [13]. It is an unconfined aquifer problem with geometry given by Figure 3, with the two angles $\alpha = 30°$ and $\beta = 15°$. The other parameters are: $K = 40$ m/day, $Q = 40$ m^2/day, and $\rho_s/\rho_f = 1.4$ (representing the density ratio in the Dead Sea.) It is noted that the boundary condition Q/Kb can not be directly applied because the thickness b is not initially known. The thickness b is updated at each iteration as the free surface and interface are adjusted.

The problem is solved by the adaptive BEM using an initial coarse mesh. The geometry and boundary conditions are described with a minimum number of nodes. Nine nodes are used for the current case (including four double nodes at the corners), which are shown as Figure 5. Such a mesh is then automatically graded through the iterations by the adaptive process. The final mesh and location of free surface and interface are depicted in Figure 6. Analyzing these two meshes, we observe that the number of nodes has increased from 9 to 40. The error tolerance used to stop the refinement process is 5×10^{-3}.

The last example is adopted from Bear and Dagan [14] following a Hele-Shaw model setup. The geometry is that of Figure 1. The parameters are: $b = 27$ cm, $K = 69$ cm/s, $\rho_s/\rho_f = 1.025$, and $Q = 3.9$ cm^2/s. The initial free interface is shown in dashed line in Figure 7. There are 11 initial nodes (including 5 double nodes) represented by square symbols. The final mesh, which contains 27 nodes shown in circle symbols, is plotted in solid line in Figure 7. The error tolerance used is 5×10^{-2}.

6 Summary and Conclusion

A numerical procedure for locating the interface and free surface in coastal aquifer saltwater intrusion has been developed. The technique involves the use of an h-adaptive BEM

43

which automatically refines the solution mesh to achieve optimal accuracy. The search for the unknown locations of free boundaries is guided by a nonlinear programming procedure. The combination of the two techniques enables an effective, automated solution procedure for saltwater intrusion problems. Several confined and unconfined aquifer problems are solved as a demonstration. Future extensions will consider the flow in the saltwater zone and aquifer heterogeneity.

Acknowledgment

Ouazar and Cheng acknowledge the partial support of the project "An intelligent integrated saltwater intrusion modeling system," through the CDR program of the U.S. Agency for International Development. Naji is supported in part by the British Council (Morocco).

References

[1] Liggett, J.A., "Location of free surface in porous media", *J. Hyd. Div., ASCE.*, **103**, 353-365, 1977.

[2] Cheng, A.H-D., Liggett, J.A. and Liu, P.L-F., "Boundary calculations of sluice and spillway flows," *J. Hyd. Div., ASCE*, **107**, 1163–1178, 1981.

[3] Liu, P.L-F., Cheng, A.H-D., Liggett, J.A. and Lee, J.H., "Boundary integral equation solutions to moving interface between two fluids in porous media," *Water Resour. Res.*, **17**, 1445–1452, 1981.

[4] Taigbenu, A.E., Liggett, J.A. and Cheng, A.H-D., "Boundary integral solution to seawater intrusion into coastal aquifers," *Water Resour. Res.*, **20**, 1150–1158, 1984.

[5] Naji, A., Ouazar, D., Wrobel, L.C. and Brebbia, C.A., "On optimization techniques for solution of free boundary problems," *Boundary Elements XIV*, Comp. Mech. Publ./Elsevier, 1992.

[6] Naji, A., Ouazar, D. and Wrobel, L.C., "Further application of optimization techniques to free boundary problems," *Boundary Elements XVI*, Comp. Mech. Publ./Elsevier, 1994.

[7] Naji, A., "Optimization techniques and h-adaptive boundary element method for free boundary value problems," Master of Philosophy thesis, Wessex Institute of Technology, University of Portsmouth, UK, 1994.

44

[8] Rencis, J.J. and Mullen, R.L. "A self adaptive mesh refinement technique for the boundary element solution of the Laplace equation," *Comput. Mech.*, **3**, 309-319, 1988.

[9] Rencis, J.J. and Jong, K.Y., "Error estimation for boundary element analysis," *J. Eng. Mech., ASCE* . 1989.

[10] Rencis, J.J. and Jong, K.Y., "A self-adaptive h-refinement technique for boundary element method," *Comp. Meth. Appl. Mech. Eng.*, **73**, 295-316, 1989.

[11] Rank, E., "Adaptive h-, p- and hp-versions for boundary integral element methods," *Int. J. Numer. Meth. Eng.*, **28**, 1335-1349, 1989.

[12] Glover, R.E., "The pattern of fresh-water flow in a coastal aquifer," In: *Sea Water in Coastal Aquifers*, H.H. Cooper, F.A. Kohout, H.R. Henry and R.E. Glover, USGS Water-Supply Paper 1613-C, C32-C35, 1964.

[13] Detournay, C. and Strack, O.D.L., "A new approximate technique for the hodograph method in groundwater flow and its application to coastal aquifers", *Water Resour. Res.*, **24**, 1471-1481, 1988.

[14] Bear, J. and Dagan, G., "Moving interface in coastal aquifers", *J. Hyd. Div., ASCE.*, **90**, 193-215, 1964.

45

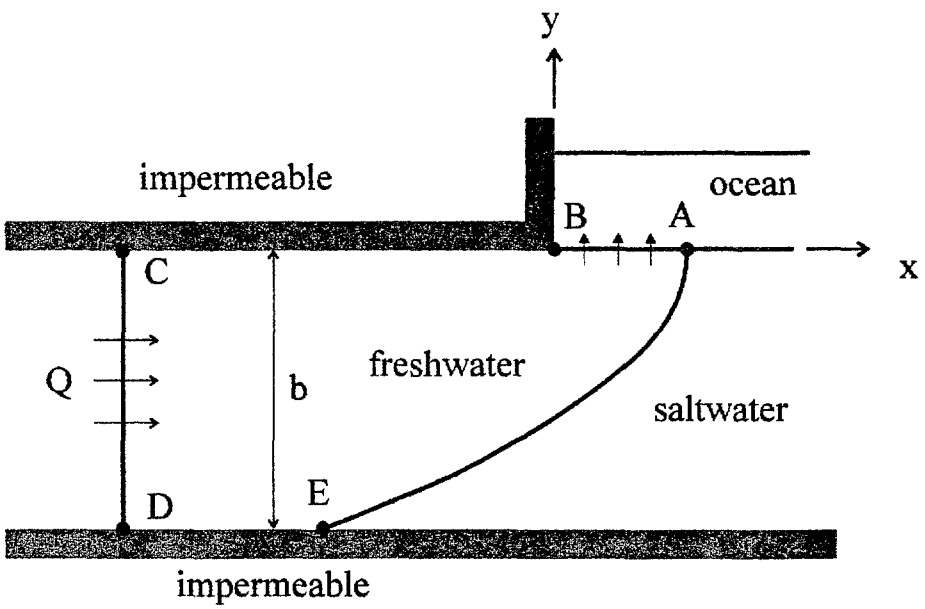

Figure 1: A confined aquifer problem.

46

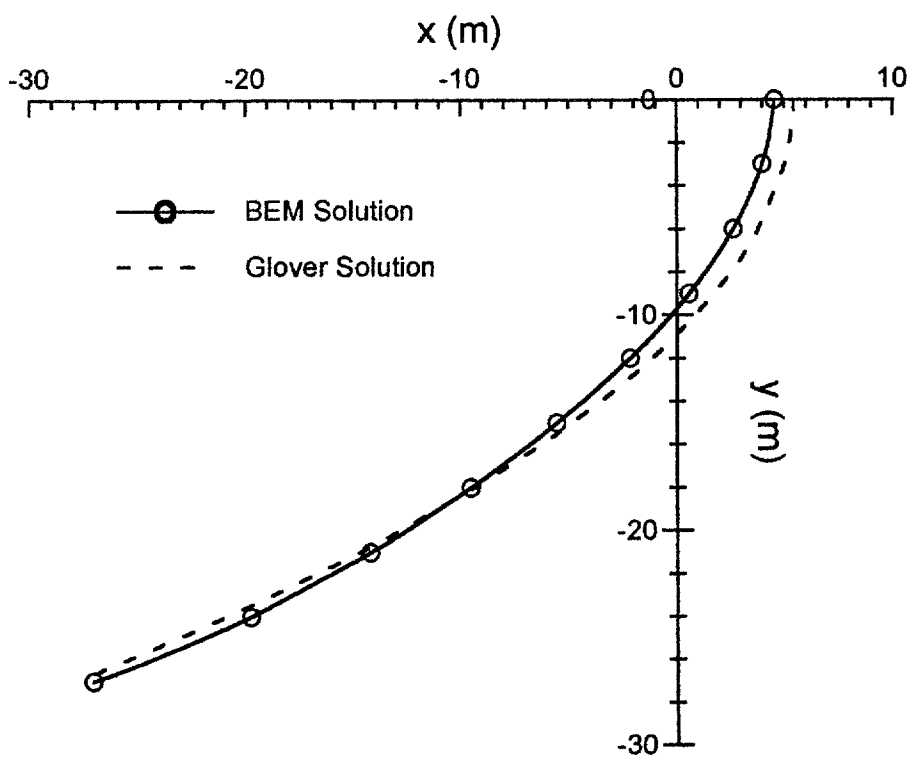

Figure 2: Final interface location of a confined aquifer problem.

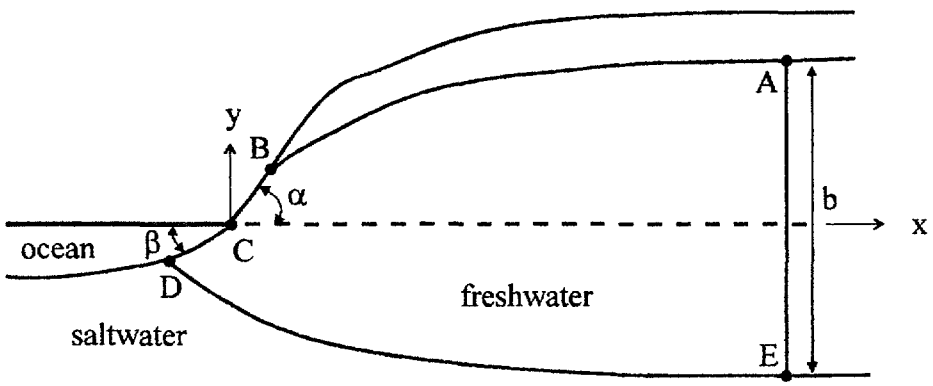

Figure 3: An unconfined aquifer problem.

48

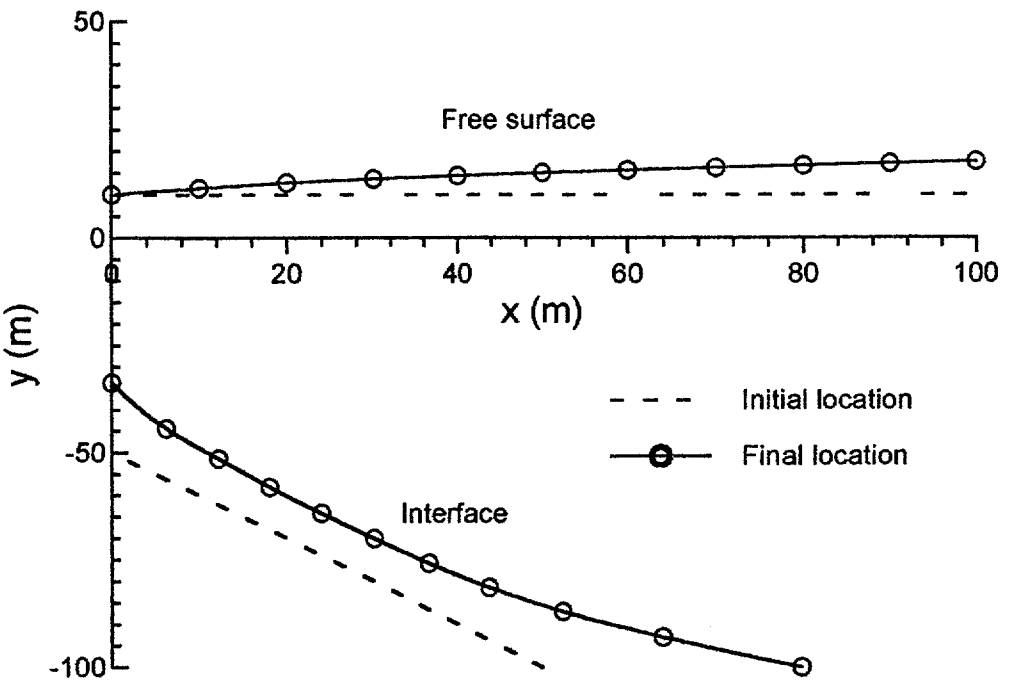

Figure 4: Free surface and interface locations of an unconfined aquifer.

- 49 -

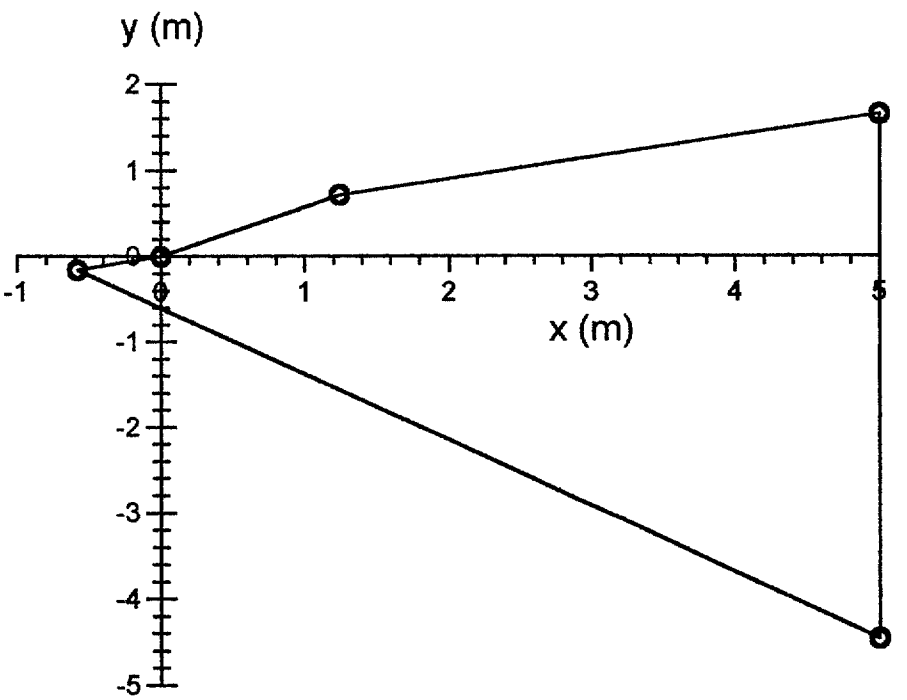

Figure 5: Initial mesh for the second unconfined aquifer problem.

50

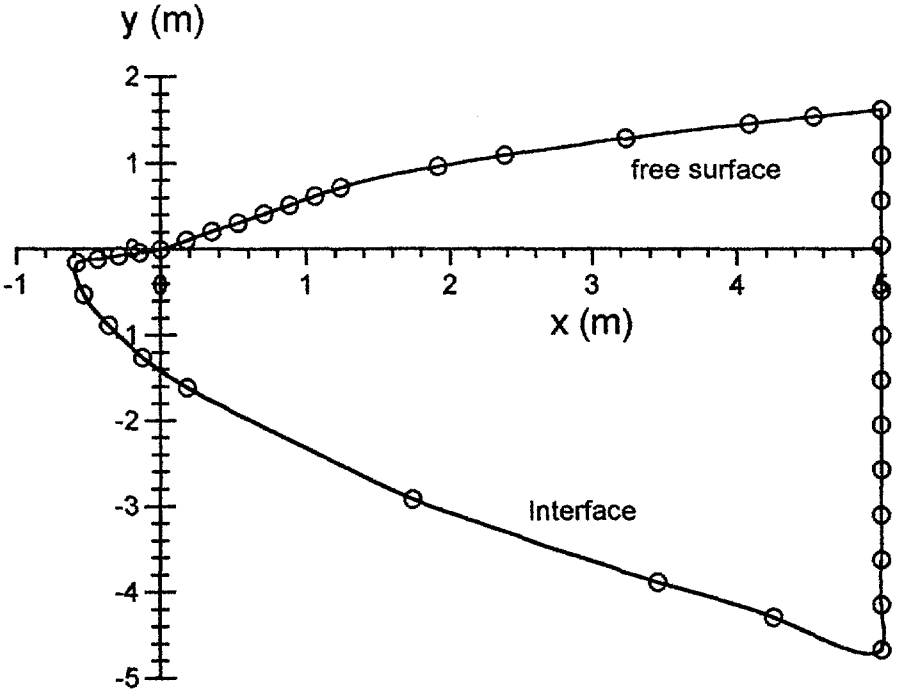

Figure 6: Final mesh and converged free surface and interface for the second unconfined aquifer problem.

51

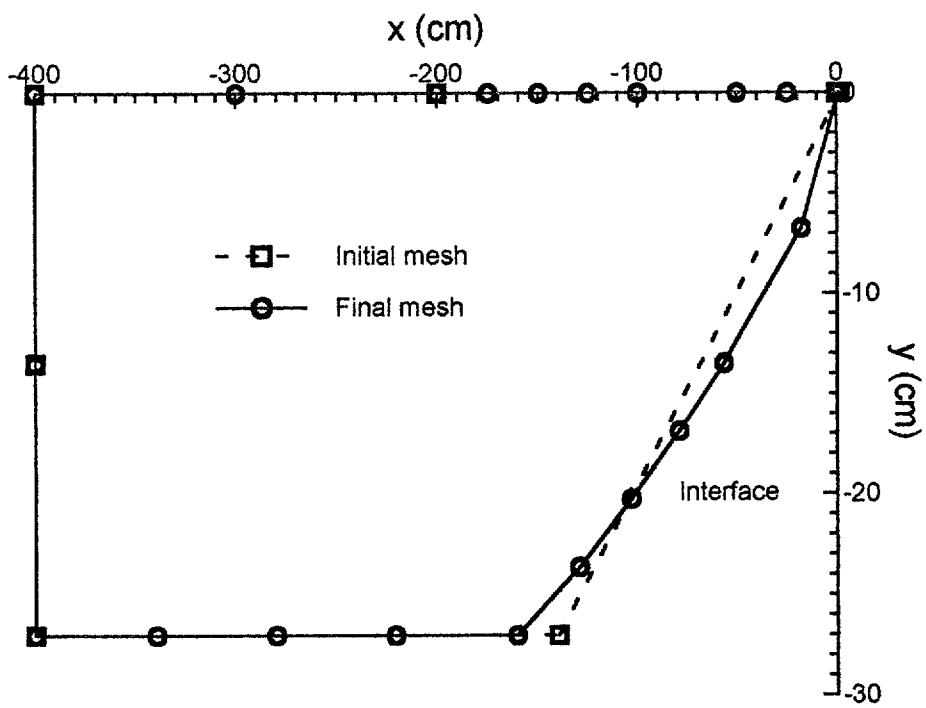

Figure 7: Initial and final mesh for the second confined aquifer problem.